HOKKAIDO UNIVERSITY

Title	RIMB-1/RIM-binding protein and UNC-10/RIM redundantly regulate presynaptic localization of the voltage-gated calcium channel in Caenorhabditis elegans.
Author(s)	Kushibiki, Yuto; Suzuki, Toshiharu; Jin, Yishi; Taru, Hidenori
Citation	The Journal of neuroscience : the official journal of the Society for Neuroscience, 39(44), 8617-8631 https://doi.org/10.1523/JNEUROSCI.0506-19.2019
Issue Date	2019-10-30
Doc URL	http://hdl.handle.net/2115/77754
Rights(URL)	https://creativecommons.org/licenses/by/4.0/
Type	article
File Information	8617.full.pdf

Instructions for use

Cellular/Molecular

RIMB-1/RIM-Binding Protein and UNC-10/RIM Redundantly Regulate Presynaptic Localization of the Voltage-Gated Calcium Channel in *Caenorhabditis elegans*

Yuto Kushibiki,[1] **Toshiharu Suzuki,**[1] **Yishi Jin,**[2] **and Hidenori Taru**[1]

[1]Laboratory of Neuroscience, Graduate School of Pharmaceutical Sciences, Hokkaido University, Sapporo 060-0812, Japan, and [2]Neurobiology Section, Division of Biological Sciences, University of California, San Diego, La Jolla, California 92093

Presynaptic active zones (AZs) contain many molecules essential for neurotransmitter release and are assembled in a highly organized manner. A network of adaptor proteins known as cytomatrix at the AZ (CAZ) is important for shaping the structural characteristics of AZ. Rab3-interacting molecule (RIM)-binding protein (RBP) family are binding partners of the CAZ protein RIM and also bind the voltage-gated calcium channels (VGCCs) in mice and flies. Here, we investigated the physiological roles of RIMB-1, the homolog of RBPs in the nematode *Caenorhabditis elegans*. RIMB-1 is expressed broadly in neurons and predominantly localized at presynaptic sites. Loss-of-function animals of *rimb-1* displayed slight defects in motility and response to pharmacological inhibition of synaptic transmission, suggesting a modest involvement of *rimb-1* in synapse function. We analyzed genetic interactions of *rimb-1* by testing candidate genes and by an unbiased forward genetic screen for *rimb-1* enhancer. Both analyses identified the RIM homolog UNC-10 that acts together with RIMB-1 to regulate presynaptic localization of the P/Q-type VGCC UNC-2/Ca$_v$2. We also find that the precise localization of RIMB-1 to presynaptic sites requires presynaptic UNC-2/Ca$_v$2. RIMB-1 has multiple FN3 and SH3 domains. Our transgenic rescue analysis with RIMB-1 deletion constructs revealed a functional requirement of a C-terminal SH3 in regulating UNC-2/Ca$_v$2 localization. Together, these findings suggest a redundant role of RIMB-1/RBP and UNC-10/RIM to regulate the abundance of UNC-2/Ca$_v$2 at the presynaptic AZ in *C. elegans*, depending on the bidirectional interplay between CAZ adaptor and channel proteins.

Key words: active zone; adaptor protein; *C. elegans*; genetic interaction; presynapse; voltage-gated calcium channel

---

Significance Statement

Presynaptic active zones (AZs) are highly organized structures for synaptic transmission with characteristic networks of adaptor proteins called cytomatrix at the AZ (CAZ). In this study, we characterized a CAZ protein RIMB-1, named for RIM-binding protein (RBP), in the nematode *Caenorhabditis elegans*. Through systematic analyses of genetic interactions and an unbiased genetic enhancer screen of *rimb-1*, we revealed a redundant role of two CAZ proteins RIMB-1/RBP and UNC-10/RIM in regulating presynaptic localization of UNC-2/Ca$_v$2, a voltage-gated calcium channel (VGCC) critical for proper neurotransmitter release. Additionally, the precise localization of RIMB-1/RBP requires presynaptic UNC-2/Ca$_v$2. These findings provide new mechanistic insight about how the interplay among multiple CAZ adaptor proteins and VGCC contributes to the organization of presynaptic AZ.

Introduction

Synapses are asymmetric cell junctional structures specialized for synaptic transmission in neurons. Neurotransmitter release from synaptic vesicles (SVs) critically depends on the active zones (AZs) at presynaptic terminals. A unique set of adaptor proteins in cytomatrix at the AZ (CAZ) interacts with each other to position AZ proteins in a highly organized manner. CAZ proteins are evolutionary conserved, and genetic studies in *Caenorhabditis*

elegans, *Drosophila*, and mouse have revealed their critical roles in presynaptic assembly and/or functions (for review, see Dresbach et al., 2001; Schoch and Gundelfinger, 2006; Südhof, 2012; Ackermann et al., 2015).

Voltage-gated calcium channel (VGCC)/voltage-dependent calcium channel (VDCC), which is composed of main pore-forming α1, ancillary β, and α2δ subunits, is one of the critical AZ molecules for synaptic transmission. In mammalian neurons, VGCC containing Ca_v2 subtype of α1, P/Q-type $Ca_v2.1$ or N-type $Ca_v2.2$, is activated in response to membrane depolarization to trigger neurotransmitter release (for review, see Simms and Zamponi, 2014). Protein binding partners of VGCC include many cytoplasmic adaptor proteins such as Rab3-interacting molecule (RIM; Kaeser et al., 2011; Wu et al., 2019), RIM-binding protein (RBP/RIM-BP; Hibino et al., 2002), ELKS (Kiyonaka et al., 2012), Cask, and Mint (Maximov et al., 1999). Loss-of-function studies have supported the requirement of RIM (Kaeser et al., 2011; Acuna et al., 2016), RBP (Acuna et al., 2015, 2016; Grauel et al., 2016), and Bassoon (Davydova et al., 2014) in mice, and RIM (Graf et al., 2012), RBP (K. S. Liu et al., 2011), Fife/RIM-Piccolo homolog (Bruckner et al., 2017), and Bruchpilot/ELKS-like protein (Kittel et al., 2006) in *Drosophila* for regulating presynaptic VGCCs.

In *C. elegans*, the *unc-2* gene encodes α1 subunit of Ca_v2 VGCC and is required for evoked neurotransmitter release (Schafer and Kenyon, 1995; Mathews et al., 2003) and tuning of presynaptic morphology at the neuromuscular junction (Caylor et al., 2013). UNC-2/Ca_v2 is concentrated at presynaptic AZ, and its localization at synapses requires endoplasmic reticulum (ER) protein CALF-1 and VGCC α2δ subunit UNC-36 for its exit from ER (Saheki and Bargmann, 2009). However, it remains unknown how other presynaptic molecules affect the presynaptic AZ localization of UNC-2/Ca_v2.

RBPs are CAZ adaptor proteins with multiple SH3 and FN3 domains, and the SH3 domains bind RIM and VGCCα1 subunits, $Ca_v2.1$, $Ca_v2.2$, and $Ca_v1.3$ (Y. Wang et al., 2000; Hibino et al., 2002; Kaeser et al., 2011; Davydova et al., 2014). Recent studies of RBP knock-out mice have revealed their roles in the regulation of presynaptic VGCC and AZ formation (Acuna et al., 2015, 2016; Grauel et al., 2016). *Drosophila* RBP is essential for the formation of AZ structure, the presynaptic localization of VGCCα1 Ca_v2 protein cacophony (Cac; K. S. Liu et al., 2011), and homeostatic modulation of neurotransmitter release (Müller et al., 2015). *C. elegans* has a single gene *rimb-1* encoding RBP family protein. Emerging evidence suggests that *rimb-1* mutants exhibit slight distribution defects of presynaptic SV and dense core vesicle (Edwards et al., 2018; Morrison et al., 2018), however, its physiological role remains unclear.

To understand the molecular mechanisms of CAZ protein network in organizing presynaptic molecules including VGCC, we have analyzed RIMB-1 in *C. elegans*. Through systematic genetic interaction study for various presynaptic and/or VGCC-binding proteins as well as an unbiased forward genetic screen, we revealed that two CAZ proteins, RIMB-1 and UNC-10/RIM, play redundant roles to regulate the abundance of presynaptic UNC-2/Ca_v2 cluster. Furthermore, our genetic and structural–functional analysis uncovered the importance of particular SH3 domain of RIMB-1 for its function and bidirectional regulation by UNC-2/Ca_v2 for the precise localization of RIMB-1.

Materials and Methods

Strains. *C. elegans* Bristol N2 and mutant strains were maintained on NGM plate seeded with *E. coli* OP50 as described previously (Brenner, 1974), and young adult hermaphrodites cultured at 20°C were used for all analyses. Mutant alleles and integrated transgenes used in this study were as follows: *lin-10(e1439)I*, *unc-13(e450)I*, *syd-1(ju2)II*, *rimb-1 (gk452845)III*, *rimb-1(gkDf40)III*, *elks-1(js816)IV*, *calf-1(ky867)V*, *rpm-1 (js410)V*, *lin-2(e1309)X*, *sad-1(ky289)X*, *syd-2(ok217)X*, *unc-2(e55)X*, *unc-10(md1117)X*, *unc-10(nq47)X*, *unc-18(e81)X*, *hpIs61[Punc-25-UNC-10-GFP]II*, *juIs76[Punc-25-GFP]II*, *juIs1[Punc-25-SNB-1-GFP]IV*, *juIs14 [Pacr-2-GFP]IV*, *hpIs5[Punc-25-SYD-2-GFP]X*, *kyIs442[Podr-3-GFP-UNC-2, Podr-3-mCherry-RAB-3]*, *kyIs479[Punc-25-GFP-UNC-2, Punc-25-mCherry-RAB-3]*, and *vaIs33[Punc-2-UNC-2-GFP]*.

Molecular biology. To generate a *rimb-1* transcriptional reporter construct, 5.1 kb genomic region upstream of ATG was amplified by PCR with YJ4630 (5′-tgccggtttttgggac-3′) and TO201 (5′-cttcacccttgaga ccatgccataggaggatgcgggggg-3′) using genomic DNA of N2 animals with Wizard SV Genomic DNA purification system (Promega) as a template. DNA fragment encoding mCherry with synthetic introns and 3′ UTR sequence of *unc-10* were amplified by PCR with TO203 (5′-atggtctca aagggtgaagaagataac-3′) and TO111 (5′-gttaatatttaaatgtttcggtattaattc-3′) using a plasmid vector pCZGY411 as a template. A single 6.3 kb fragment with P*rimb-1*-mCherry-*unc-10* 3′ UTR was generated using these two partially overlapped fragments for PCR amplification. RIMB-1 cDNAs were obtained by RT-PCR with PrimeScriptII RT-PCR Kit (Takara Bio) and PrimeSTAR Max DNA polymerase (Takara Bio) using total RNA purified from N2 with ISOGEN (Nippon Gene). In detail, RIMB-1a cDNA (NM_065058_3) was amplified with TO372 (5′-agcaggctccgaattcggc atgctggcggtctgtcg-3′) and TO382 (5′-aagctgggtcgaatttaaattatccttttt tctttgcaccgg-3′). RIMB-1b cDNA clone was obtained by nested PCR using specific primers designed for the both ends of predicted *tag-168* coding sequence (NM_065058_1): TO223 (5′-tatggcatggtgccaggcccgtcg acctcgttcac-3′) and TO224 (5′-ttccggcgatttatcgatttacccacggattatcg-3′) for the first reaction, and TO227 (5′-agcaggctccgaattcggcatggtgccagg cccgt-3′) and TO228 (5′-aagctgggtcgaattcttatcgatttacccacgga-3′) for the second nested reaction. These PCR products were subcloned into Gateway entry vector pCR8 digested with EcoRI using Gibson Assembly Master Mix (New England Biolabs) or In-Fusion HD Cloning System (Takara Bio) to create pTR259 (pCR8-RIMB-1a) or pTR179 (pCR8-RIMB-1b). The rimb-1b fragment containing putative entire coding sequence was amplified with TO372 and TO380 (5′-aagctgggtcgaatttaaa ttatcgatttacccacggattatcg-3′) and the sequence was deposited on the public database (GenBank, MK431866). Entry clones of RIMB-1 deletion constructs were generated based on pTR179 as follow: for pTR255 (pCR8-RIMB-1ΔSH3-III), pTR179 was digested with SacI and self-ligated. For pTR256 (pCR8-RIMB-1ΔC), pTR179 was digested with SacI and SacII, and treated with T4 DNA polymerase (Nippon Gene) to create blunt ends, and self-ligated. For pTR254 (pCR8-RIMB-1ΔN) a fragment including vector backbone was amplified by PCR with TO363 (5′-atcatcatgcctcctctagacc-3′) and TO364 (5′-gatgcgactgcggctctagagcgagaa ttgggtctcgaacg-3′) using pTR179 as template, the other 2.9 kbp RIMB-1 fragment was cut from pTR179 by XbaI digestion, and these two fragments were assembled using Gibson assembly. All these cDNAs and constructs were checked by sequencing with 3130xl Genetic Analyzer and BigDye Terminator v3.1 (Applied Biosystems). Expression vectors were basically generated using Gateway LR Clonase II Enzyme mix (Thermo-Fisher Scientific) from entry clones as mentioned above. pCZGY396 and pCZGY60 destination vectors were used for expressions of N-terminally mCherry fused proteins in D-type motor neuron under *unc-25* promoter and of N-terminally FLAG-tagged proteins under pan-neuronal *rgef-1* promoter (Taru and Jin, 2011), respectively.

Transgenics. Transgenic animals were generated by microinjection as described previously (Mello et al., 1991). Multiple transgenic lines were obtained and analyzed unless otherwise noted. DNA materials and the corresponding allele numbers for representative extrachromosomal arrays were as follows: for transcriptional reporter P*rimb-1*-mCherry, 7.8 ng/μl of PCR fragment of P*rimb-1*-mCherry-*unc-10* 3′ UTR and 40 ng/μl of coinjection marker pRF4 were injected into wild-type animals for *nqEx62*. For pan-neuronal overexpression of RIMB-1 constructs, 10 ng/μl of each plasmid with 90 ng/μl of coinjection marker P*ttx-3*-GFP or P*ttx-3*-RFP were injected into *rimb-1(gk452845); unc-10(md1117); kyIs479* animals: pTR1001 (P*rgef-1*-FLAG-RIMB-1b) for

nqEx63, pTR1011 (P*rgef-1*-FLAG-RIMB-1a) for *nqEx89*, pTR1002 (P*rgef-1*-FLAG-RIMB-1bΔN) for *nqEx76*, pTR1004 (P*rgef-1*-FLAG-RIMB-1bΔC) for *nqEx80*, and pTR1003 (P*rgef-1*-FLAG-RIMB-1bΔSH3-III) for *nqEx79*. For the expression of mCherry-RIMB-1 constructs in D neurons, 20 ng/μl of each plasmid with 50 ng/μl of coinjection marker P*ttx-3*-GFP were injected into wild-type animals with or without *juIs1* transgene: pTR1012 (P*unc-25*-mCherry-RIMB-1a) for *nqEx84*, pTR185 (P*unc-25*-mCherry-RIMB-1b) for *nqEx41*, pTR1007 (P*unc-25*-mCherry-RIMB-1bΔN) for *nqEx71*, pTR1009 (P*unc-25*-mCherry-RIMB-1bΔC) for *nqEx72*, and pTR1008 (P*unc-25*-mCherry-RIMB-1bΔSH3-III) for *nqEx82*. For the other analyses, *nqEx63*, *nqEx41*, and *nqEx84* were introduced into various mutant or transgenic marker backgrounds by genetic crosses.

Genetic screening of rimb-1 *enhancer.* rimb-1(gk452845); kyIs442 were mutagenized with ethyl methanesulfonate as described previously (Brenner, 1974). F2 animals with severe uncoordinated movement phenotype were examined under fluorescent microscopes for abnormal GFP-UNC-2 localization in AWC neurons. From the screening of ~5000 haploid genomes, a mutant allele *nq47* was isolated with a strong enhanced GFP-UNC-2 localization phenotype. Conventional genetic linkage and complementation analyses were performed to identify *unc-10* as affected by *nq47*. 9.5 kb genomic region including the entire *unc-10* gene was amplified by PCR and sequenced with BGISEQ-500 (BGI Genomics).

Live imaging. Live animals were placed on 5% agar pads and immobilized with 1% 1-phenoxy-2-propanol (Wako) in M9 buffer (22 mM KH₂PO₄, 41 mM Na₂HPO₄, 9 mM NaCl, 19 mM NH₄Cl) to observe D neurons, or with 1 mM levamisole (Wako) in M9 buffer to observe AWC neurons. All images were obtained on an inverted fluorescent microscope (Keyence, BZ-X710) using a 60× NA 1.20 water (Nikon, CFI Plan Apochromat VC) or 100× NA 1.45 oil (Nikon, CFI Plan Apochromat Lambda) for synaptic protein markers, and a 20× NA 0.45 air (Nikon, CFI S Plan Fluor ELWD) or the 60× objective for transcriptional reporters. Fluorescence signals were filtered using BZ-X filter GFP OP-87763 and TRITC OP-87764 (Keyence) and commonly adjusted using Haze Reduction application (Keyence). To draw line-scan intensity profiles, the fluorescence intensity in each pixel along neurites was measured using Line-Profile command in Keyence application (Keyence), and was graphically displayed using Microsoft Excel.

Quantification of fluorescence markers. Quantification of GFP-UNC-2 and mCherry-RAB-3 signals in AWC axon was performed as follows: Images were captured using the 100× objective for two focal planes for each animal to cover the Z-depth of presynaptic region and subjected to Haze Reduction. Using ImageJ (National Institutes of Health), absolute threshold value, with which the signal of GFP-UNC-2 or mCherry-RAB-3 puncta was appropriately extracted from the image, was determined in the pilot analysis of wild-type samples and commonly applied to all images of various strains. Then, Analyze Particle command was performed to measure total area, number, and average size of the fluorescence puncta. GFP areas within the axonal region marked with mCherry-RAB-3 were quantified and normalized by neurite length. To measure total fluorescence of GFP-UNC-2 in axon and make a 3D heatmap of fluorescence intensity, background signal was linearly subtracted from each original image using Line-Profile and Black Balance commands in Keyence application. Then, resulting images were analyzed by integrated density for total GFP fluorescent signal along axons and visualize by Interactive 3D Surface Plot plugin using ImageJ. Mean value of two focal planes for each animal was indicated as a ratio to wild type and used for the statistical analysis.

Quantification of GFP-UNC-2 and SNB-1-GFP fluorescence signals in D neurons was performed as follows: images for GFP-UNC-2 were captured using the 100× objective and subjected to haze reduction, and those for SNB-1-GFP were captured using the 60× objective. A single focal plane image, in which presynaptic markers were appropriately focused over 40 μm along neurite, was selected for each worm. GFP-UNC-2 or SNB-1-GFP puncta were manually identified based on consistent criteria and counted by a single observer. The number of puncta per 100 μm was calculated and used for statistical analysis.

Immunohistochemistry. Whole-mount staining of adult worms *vaIs33* [P*unc-2*-UNC-2-GFP]; *nqEx63*[P*rgef-1*-FLAG-RIMB-1b] was performed based on a Finney–Ruvkun's protocol (Finney and Ruvkun, 1990) except that 2% formaldehyde was used for fixation. The samples were rotated with primary antibodies in AbA buffer at 4°C overnight and with secondary antibodies in AbA for 4 h at room temperature. The monoclonal mouse antibody M2 against FLAG (Sigma-Aldrich, F1804) was used at 1 μg/ml, and the polyclonal rabbit antibody against GFP (MBL, 598) was used at 1:1000 dilution. AlexaFluor 647-conjugated goat anti-mouse IgG (Abcam, A-21235) and AlexaFluor 488-conjugated donkey anti-rabbit IgG (Abcam, A-21206) secondary antibodies were used at 1 μg/ml. Worms were mounted on the 5% agar pad, and images of dorsal nerve cords were captured on an inverted fluorescence microscope (BZ-X710, Keyence) using a 100× NA 1.45 oil (Nikon, CFI Plan Apochromat Lambda) immersion objective, and BZ-X filter GFP OP-87763 or Cy5 OP-87766 (Keyence).

Behavioral analyses. For swimming assay, young adult worms (24 h after late L4 stage, 9–20 animals for each strain) were put into a drop of M9 buffer on top of an NGM plate and counted body bends for 2 min after a 30 s recovery period. For aldicarb assay, 80 young adult worms (24 h after late L4 stage) were transferred to OP50 seeded two NGM plates containing 1 mM aldicarb (AccuStandard), and paralyzed animals were counted every 40 min for 8 h. Animals that crawled off the plates were excluded from the analysis. In both assays, strains were scored in parallel, with the researcher blinded to genotype, and two independent experiments reproduced the same trend.

Experimental design and statistical analysis. All experiments were performed using young adult hermaphrodites of *C. elegans* Bristol N2 and its derived strains. All quantitative data were reported as mean ± SD, and *n* indicated the number of animals. One-way ANOVA was applied for the analyses of swimming and fluorescence imaging followed by *post hoc* tests as described below: Tukey–Kramer tests for Figures 2F, 3F, and SNB-1-GFP quantification in Table 1; Tukey tests for Figures 2A, 4K–N, and GFP-UNC-2 and mCherry-RAB-3 quantification in Table 1; and Dunnett test for Figure 5B were performed. Two-tailed Student's *t* test was applied for the comparisons of SNB-1-GFP puncta number between wild type and *rimb-1*. For the survival analyses in Figure 2, *B* and *H*, log rank tests were performed, and adjusted *p* values using Bonferroni correction were indicated. All statistics were performed using JMP (SAS Institute), and all graphs were made using Prism 5 (GraphPad Software).

Results

RIMB-1 is a pan-neuronal presynaptic AZ protein

C. elegans rimb-1, formally named as *tag-168*, is predicted to produce multiple isoforms on NCBI database. We performed RT-PCR to verify mRNAs expressed and isolated two alternative splicing isoforms, designated as *rimb-1a* and *rimb-1b*, which encode almost identical proteins with slightly different amino-acid sequences at the C-terminal end (Fig. 1A). *rimb-1a* is more dominantly expressed isoform than *rimb-1b* based on the RNA sequence data (https://wormbase.org). Both RIMB-1 proteins have three SH3 and two FN3 domains, with one SH3 domain (SH3-I) at the N-terminus followed by two FN3 domains (FN3-I and -II) and two tandem SH3 domains (SH3-II and -III) located in the C-terminal region (Fig. 1A), similar to the domain composition of RBP family proteins in other species. *C. elegans* RIMB-1a has 34 and 33% overall amino-acid identity to mouse RBP2 and *Drosophila* RBP proteins, respectively.

RBPs in mice and flies are localized to presynaptic AZs (Hibino et al., 2002; K. S. Liu et al., 2011; Davydova et al., 2014; Siebert et al., 2015). Neural expression of worm *rimb-1* is suggested by transcriptomic analysis data (https://wormbase.org), and its upstream region has been used as a promoter for pan-neuronal expression (Macosko et al., 2009). We also expressed mCherry protein under 5.1 kb genomic region upstream of the *rimb-1* coding sequence and observed red fluorescent signal exclusively in the nervous system (Fig. 1B), including head and tail ganglia (Fig. 1C,D), and dorsal and ventral nerve cords (Fig. 1E).

Table 1. Quantitative results of the double loss-of-function mutant analyses of *rimb-1*

			AWC sensory neuron				D motor neuron	
			GFP-UNC-2		mCherry-RAB-3		SNB-1-GFP	
			Total puncta area; relative ratio to WT		Total puncta area; relative ratio to WT		No. puncta/100 μm	
Gene	Allele	Genotype	Mean ± SD	Statistics	Mean ± SD	Statistics	Mean ± SD (n)	Statistics
		Wild type	1.00 ± 0.58		1.00 ± 0.48		19.9 ± 2.5 (11)	
rimb-1/RBP	*gk452845*	rimb-1(gk452845)	1.06 ± 0.61		1.65 ± 0.48		19.8 ± 2.1 (11)	
	gkDf40[¶,‖]	rimb-1(gkDf40)	1.16 ± 0.64		2.09 ± 0.90*		18.3 ± 1.9 (11)	
unc-10/RIM	*md1117*[¶]	unc-10	0.78 ± 0.42		2.47 ± 0.90*		19.8 ± 2.0 (15)	
		unc-10; rimb-1(gk452845)	0.07 ± 0.08§	$F_{(3,36)} = 8.49, p = 0.0002$	2.16 ± 0.74	$F_{(3,36)} = 10.24, p < 0.0001$	18.1 ± 2.8 (15)	$F_{(3,48)} = 1.77, p = 0.17$
		unc-10; rimb-1(gkDf40)	0.07 ± 0.06§	$F_{(3,36)} = 9.09, p = 0.0001$	2.37 ± 0.75	$F_{(3,36)} = 8.06, p = 0.0003$	18.3 ± 1.9 (13)	$F_{(3,46)} = 2.05, p = 0.12$
syd-2/Liprinα	*ok217*[¶]	syd-2	1.14 ± 0.55		1.44 ± 1.51		20.4 ± 4.7 (10)	
		syd-2; rimb-1(gk452845)	1.09 ± 0.40	$F_{(3,36)} = 0.10, p = 0.96$	1.35 ± 1.35	$F_{(3,36)} = 0.58, p = 0.63$	20.4 ± 4.3 (16)	$F_{(3,44)} = 0.21, p = 0.89$
unc-13/Munc13	*e450*	unc-13	0.91 ± 0.39		1.55 ± 0.55		21.0 ± 2.1 (18)	
		unc-13; rimb-1(gk452845)	0.69 ± 0.37	$F_{(3,36)} = 0.95, p = 0.43$	1.26 ± 0.69	$F_{(3,36)} = 2.51, p = 0.074$	18.0 ± 3.0 (14)†	$F_{(3,50)} = 3.70, p = 0.018$
elks-1/ELKS	*js816*[¶]	elks-1	1.54 ± 0.47		2.09 ± 0.60*		21.0 ± 3.1 (10)	
		elks-1; rimb-1(gk452845)	1.45 ± 0.45	$F_{(3,36)} = 2.34, p = 0.09$	2.44 ± 0.49	$F_{(3,36)} = 13.17, p < 0.0001$	19.4 ± 3.2 (14)	$F_{(3,42)} = 0.67, p = 0.58$
syd-1/RhoGAP-like	*ju2*[¶]	syd-1	1.12 ± 0.42		0.94 ± 0.35		19.6 ± 2.8 (12)	
		syd-1; rimb-1(gk452845)	1.03 ± 0.35	$F_{(3,36)} = 0.10, p = 0.96$	2.12 ± 0.65††	$F_{(3,36)} = 11.46, p < 0.0001$	20.2 ± 4.3 (13)	$F_{(3,43)} = 0.084, p = 0.97$
rpm-1/E3 ligase	*js410*[¶]	rpm-1	0.76 ± 0.32		2.03 ± 0.48*		16.2 ± 2.2 (12)*	
		rpm-1; rimb-1(gk452845)	0.93 ± 0.23	$F_{(3,36)} = 0.70, p = 0.56$	1.54 ± 0.42	$F_{(3,36)} = 7.51, p = 0.0005$	15.3 ± 2.3 (17)	$F_{(3,47)} = 13.01, p < 0.0001$
sad-1/SAD kinase	*ky289*	sad-1	1.09 ± 0.58		1.38 ± 1.00		20.2 ± 3.0 (12)	
		sad-1; rimb-1(gk452845)	1.38 ± 1.44	$F_{(3,36)} = 0.32, p = 0.81$	1.46 ± 0.86	$F_{(3,36)} = 1.22, p = 0.32$	16.5 ± 3.1 (11)††	$F_{(3,41)} = 4.05, p = 0.013$
unc-2/VGCCα1	*e55*[¶]	unc-2	NA		NA		19.9 ± 1.7 (14)	
		unc-2; rimb-1(gk452845)	NA		NA		20.3 ± 2.4 (10)	$F_{(3,42)} = 0.10, p = 0.96$
unc-18/Munc18	*e81*	unc-18	1.27 ± 0.36		2.32 ± 0.41*		20.5 ± 3.4 (12)	
		unc-18; rimb-1(gk452845)	1.24 ± 0.53	$F_{(3,36)} = 0.58, p = 0.64$	2.54 ± 1.03	$F_{(3,36)} = 10.41, p < 0.0001$	16.6 ± 3.4 (12)†	$F_{(3,42)} = 3.94, p = 0.015$
lin-2/CASK	*e1309*	lin-2	1.25 ± 0.66		1.19 ± 0.33		21.7 ± 2.5 (16)	
		lin-2; rimb-1(gk452845)	1.19 ± 0.31	$F_{(3,36)} = 0.39, p = 0.76$	2.09 ± 0.60††	$F_{(3,36)} = 9.24, p = 0.0001$	17.8 ± 1.9 (11)†	$F_{(3,45)} = 5.89, p = 0.0018$
lin-10/Mint	*e1439*[¶]	lin-10	1.50 ± 0.62		1.62 ± 0.84		21.0 ± 2.6 (15)	
		lin-10; rimb-1(gk452845)	1.72 ± 0.56	$F_{(3,36)} = 3.03, p = 0.042$	2.17 ± 0.60	$F_{(3,36)} = 5.43, p = 0.0035$	20.0 ± 2.6 (11)	$F_{(3,44)} = 0.65, p = 0.59$

Double loss-of-function mutants of *rimb-1* were analyzed for the distribution of presynaptic UNC-2/Ca$_v$2 and SV markers. The total area of coexpressed GFP-UNC-2 and mCherry-RAB-3 puncta in the axons of AWC neurons ($n = 10$) and the number of SNB-1-GFP puncta along the dorsal cords of D neurons ($n = 10$–18 as indicated) were quantified. Candidate genes and alleles used in the analyses are listed on the left. For each candidate mutant allele, statistical comparisons among four strains (wild type, *rimb-1*, single mutant, double mutant with *rimb-1*) were performed by one-way ANOVA. The presence of significant differences ($p < 0.05$) in subsequent *post hoc* Tukey or Tukey–Kramer test in the following comparisons is indicated: *, single mutant versus wild type; †, double mutant versus single mutant; ††, double mutant versus both single mutant and wild type; §, double mutant versus all three other strains; NA, Not applicable; ¶, protein or functional null alleles; ‖, *gkDf40* is a large deletion lacking multiple genes including *rimb-1*.

We analyzed the subcellular localization of RIMB-1 protein in D-type motor neurons (D neurons). D neurons are a set of GABAergic motor neurons, with their cell bodies located in the ventral nerve cord and their axons innervate dorsal and ventral muscles (White et al., 1986). Dorsal D (DD) neurons form presynaptic sites that are evenly distributed along axons on the dorsal side (Fig. 1F), whereas ventral D neurons form the presynaptic sites on the ventral side. RIMB-1 isoforms were expressed as mCherry-fusion protein under *unc-25* promoter specific for GABAergic neurons. mCherry-RIMB-1a and RIMB-1b displayed identical localization pattern, seen as evenly distributed small puncta along both dorsal and ventral nerve cords. To characterize this punctate localization, mCherry-RIMB-1 was coexpressed with transgenic SV marker GFP-labeled SNB-1/VAMP2 in D neurons. Most of the small bright mCherry-RIMB-1a spots were found within the puncta of SNB-1-GFP (Fig. 1G). Moreover, mCherry-RIMB-1a puncta resembled those of GFP-labeled presynaptic AZ protein UNC-10/RIM (Koushika et al., 2001), and mostly colocalized with UNC-10-GFP (Fig. 1H). mCherry-RIMB-1b displayed the same colocalization pattern with SNB-1-GFP and UNC-10-GFP. Together, these observations suggest that RIMB-1 is pan-neuronally expressed protein, and mainly localized to AZs in presynaptic sites.

Loss of RIMB-1 causes mild neuronal dysfunction

To address the physiological functions of *rimb-1*, we analyzed a mutant allele *gk452845*, which introduces a premature stop codon within the exon encoding the first SH3 domain and, therefore, likely causes strong loss-of-function (Fig. 1A). *rimb-1(gk452845)* mutant animals were morphologically normal and displayed wild-type-like movement on culture plates. When their motility was analyzed by swimming assay, the *rimb-1* mutants displayed fewer frequencies of body bending than wild-type control (Fig. 2A, *rimb-1*), suggesting a decreased motility. We also examined transgenic overexpression animals, in which RIMB-1b tagged with FLAG at the N-terminus was expressed under a pan-neuronal *rgef-1* promoter. The RIMB-1 transgenic animals in wild-type background behaved normally on culture plates and in swimming assay (Fig. 2A, *Ex[RIMB-1]*). When the RIMB-1 transgene was introduced in the *rimb-1(gk452845)* mutants, decreased body bending observed in the mutant was restored close to the level of wild type (Fig. 2A, *rimb-1;Ex[RIMB-1]*; one-way ANOVA: $F_{(3,76)} = 30.34$, $p < 0.0001$, *post hoc* Tukey's tests: $p < 0.0001$ for wild type vs *rimb-1*, $p = 0.16$ for wild type vs *Ex[RIMB-1]*, $p = 0.0018$ for wild type vs *rimb-1; Ex[RIMB-1]*, $p < 0.0001$ for *rimb-1* vs *Ex[RIMB-1]*, $p < 0.0001$ for *rimb-1* vs *rimb-1; Ex[RIMB-1]*, $p = 0.35$ for *Ex[RIMB-1]* vs *rimb-1; Ex[RIMB-1]*). These results suggest that the *rimb-1(gk452845)* mutation causes mild motility defect due to loss of RIMB-1 function in neurons.

To ask whether the *rimb-1* mutation impairs synaptic function, we examined the sensitivity to acetylcholine esterase inhibitor aldicarb, which is commonly used to estimate the activity of synaptic transmission in worms (Nguyen et al., 1995). Treatment of worms with aldicarb causes acute paralysis due to the accumulation of neurotransmitter acetylcholine, while the animals with decreased synaptic transmission in cholinergic neurons are resistant to aldicarb. Upon aldicarb treatment, *rimb-1* mutants sur-
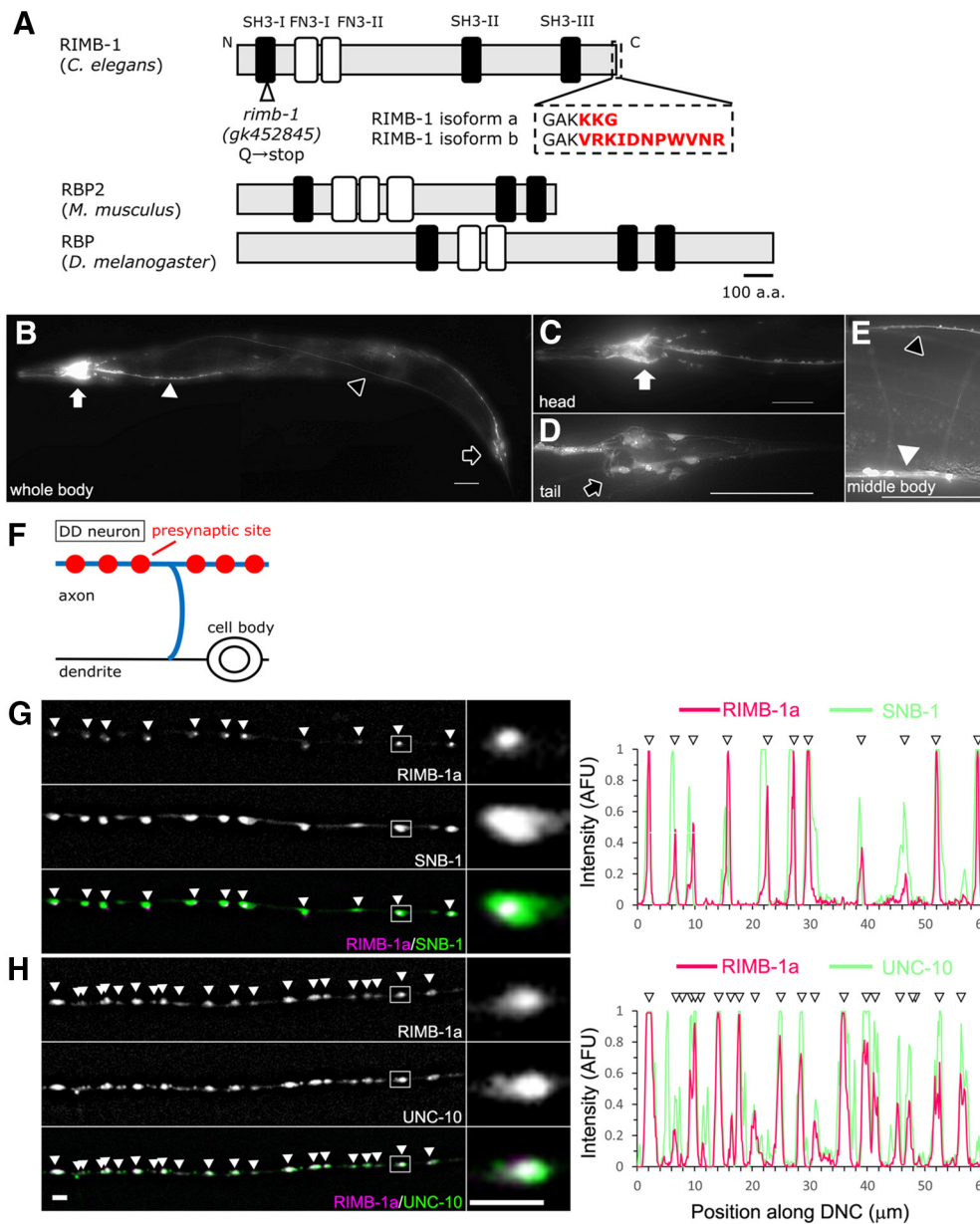
Figure 1. RIMB-1 is the *C. elegans* RBP family protein localized at presynaptic AZ. **A**, Schematic presentation of RBP family proteins, which have three SH3 (black rectangles) and two or three FN3 (white rectangles) domains. Worm RIMB-1a and RIMB-1b isoforms have different amino acid sequences at the C-terminal end. *rimb-1(gk452845)* allele introduces a premature stop codon as indicated. **B–E**, Expression pattern of *rimb-1* transcriptional reporter. Representative fluorescent images of transgenic animals expressing mCherry under *rimb-1* promoter region. mCherry signal was detected broadly in neurons, including head ganglion (**B**, **C**, white arrows), tail ganglion (**B**, **D**, black arrows), dorsal nerve cord (**B**, **E**, black arrowheads), and ventral nerve cord (**B**, **E**, white arrowheads). Scale bars, 50 μm. **F**, Schematic drawing of a dorsal D-type motor neuron. Presynaptic structures (red circles) are formed along the dorsal cord in a DD neuron. **G**, **H**, Localization of mCherry-RIMB-1a coexpressed with GFP-tagged SV protein SNB-1/VAMP2 (**G**) or AZ protein UNC-10/RIM (**H**) in D neurons. Representative fluorescent images of dorsal cords (left), enlarged view of the boxed single presynaptic site (middle), and corresponding line scan intensity profiles of mCherry-RIMB-1a (magenta) and SNB-1-GFP or GFP-UNC-10 (green) signals along axon (right) are shown. Scale bars, 2 μm. AFU, Arbitrary fluorescence unit; DNC, dorsal nerve cord. Regularly distributed mCherry-RIMB-1 puncta (arrowheads) were colocalized with both presynaptic protein markers.

vived significantly longer than wild type (Fig. 2B, *rimb-1*), suggesting *rimb-1* mutation caused mild impairment of synaptic transmission. Contrary, pan-neuronal RIMB-1 overexpression in wild-type background made the animals more sensitive to aldicarb (Fig. 2B, *Ex[RIMB-1]*). *rimb-1* mutants with the RIMB-1 transgene were more sensitive to aldicarb treatment than wild-type or *rimb-1* mutants, similar to RIMB-1 transgenic animals in wild-type background (Fig. 2B, *rimb-1;Ex[RIMB-1]*; log rank test, χ^2: 121.89, $p < 0.0001$, comparing each groups: $p < 0.0001$ for wild type vs *rimb-1*, $p < 0.0001$ for wild type vs *Ex[RIMB-1]*,

$p < 0.0001$ for wild type vs *rimb-1; Ex[RIMB-1]*, $p < 0.0001$ for *rimb-1* vs *Ex[RIMB-1]*, $p < 0.0001$ for *rimb-1* vs *rimb-1; Ex[RIMB-1]*, $p = 0.56$ for *Ex[RIMB-1]* vs *rimb-1; Ex[RIMB-1]*). These results suggest that pan-neuronal RIMB-1 overexpression enhances synaptic transmission, while it is not sufficient to induce hyperactivity in the motility assay, and rescues the defect in *rimb-1* mutants. Together these phenotypes of the *rimb-1* loss-of-function mutant and transgenic overexpression animals suggest that neuronal RIMB-1 is involved in synaptic function, although it is not critical.
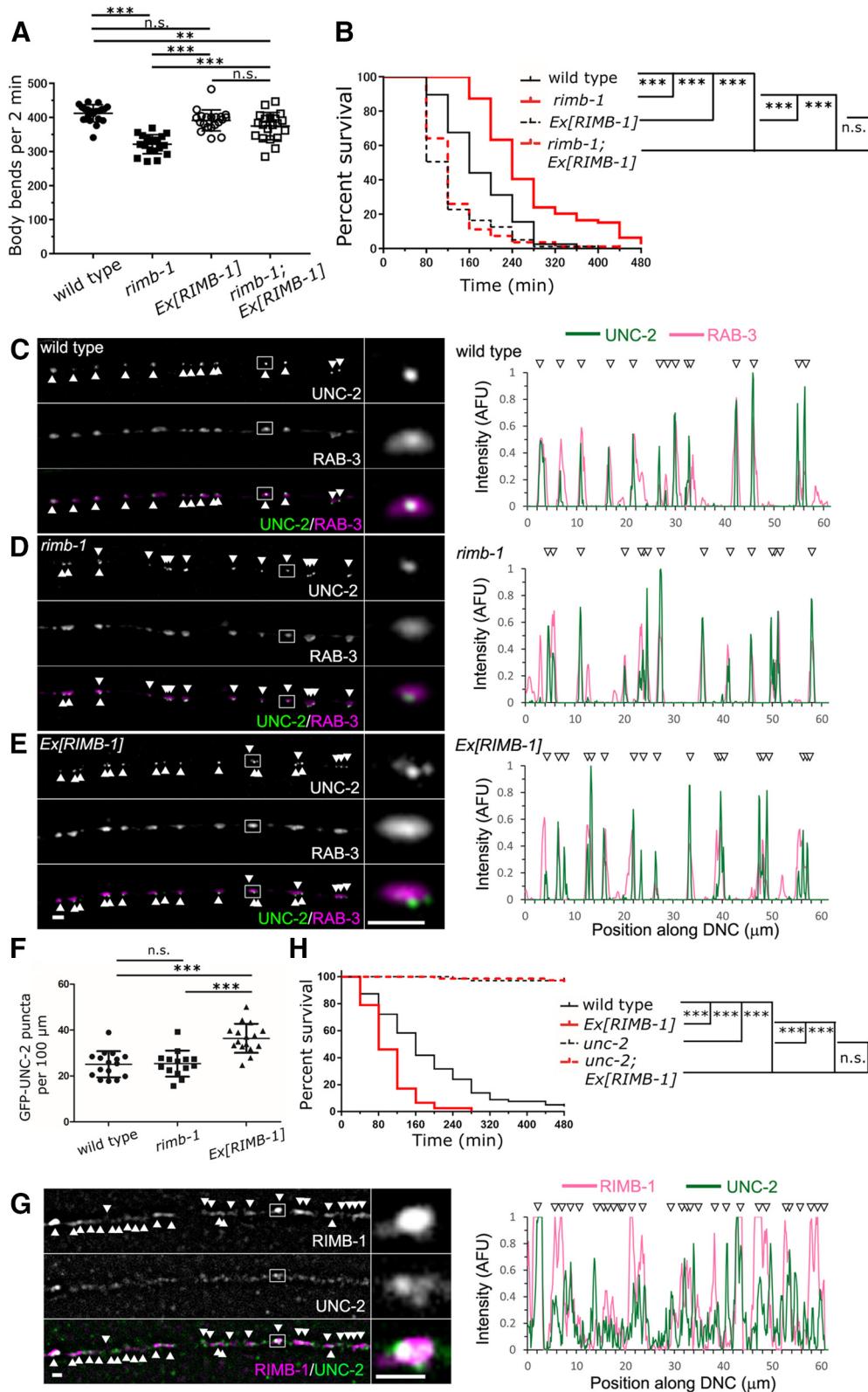
Figure 2. Effects of loss or overexpression of RIMB-1 on neuronal functions and presynaptic localization of UNC-2/Ca$_v$2. **A**, Swimming motilities of *rimb-1* mutants and transgenic animals pan-neuronally overexpressing RIMB-1b (*Ex[RIMB-1]*). *rimb-1* mutants displayed fewer body bends, and the RIMB-1 overexpression restored the defect. Mean ± SD, $n = 20$. Tukey test following one-way ANOVA: n.s. $p \geq 0.05$, **$p < 0.01$, ***$p < 0.001$. **B, H**, Survival rates upon treatment with aldicarb. *rimb-1* mutants were less sensitive to aldicarb (**B**), and the RIMB-1 overexpression increased the sensitivity in wild type (**B, H**) and *rimb-1* (**B**) but not in *unc-2* mutant background (**H**). $n = 70 – 80$. Log rank test with Bonferroni correction: n.s, $p \geq 0.05$, ***$p < 0.001$. **C–E**, Localization of GFP-UNC-2 coexpressed with mCherry-RAB-3 in D neurons was analyzed in wild type (**C**), *rimb-1* mutants (**D**), and the RIMB-1 transgenic animals (**E**). GFP-UNC-2 was observed as small puncta (arrowheads) colocalized with mCherry-RAB-3. **F**, Quantification of the number of GFP-UNC-2 puncta in D neurons. The RIMB-1 transgenic animals had more GFP-UNC-2 puncta. Mean ± SD, $n = 14 – 16$. Tukey–Kramer test following one-way ANOVA: n.s. $p \geq 0.05$, ***$p < 0.001$. **G**, Immunostaining of FLAG-RIMB-1 and GFP-UNC-2 expressed under pan-neuronal and *unc-2* promoters, respectively. RIMB-1 staining (arrowheads) overlapped with UNC-2 staining. All fluorescent images are representative of dorsal cords (left) and enlarged view of the boxed regions (middle) accompanied with line scan intensity profiles along the nerve cords (right charts). Scale bars, 2 μm.

Loss of RIMB-1 does not obviously impair the distribution of presynaptic proteins

Loss of *rimb-1* function does not affect the gross neuronal morphology as observed using transgenic GFP reporter expressed in GABAergic D-type and cholinergic A/B-type motor neurons. Because RIMB-1 was localized to presynaptic sites, we explored presynaptic phenotypes of the *rimb-1* mutants using transgenic fluorescence markers expressed in D neurons. Distribution of presynaptic SV marker SNB-1-GFP was mostly normal in *rimb-1* mutant axons. The number of puncta was comparable to that in wild type (19.9 ± 2.5 and 19.8 ± 2.1 per 100 μm dorsal nerve cords in wild type and *rimb-1*, respectively; mean $\pm$ SD, $n = 11$. two-tailed Student's t test: $t_{(20)} = 0.10$, $p = 0.92$) and we also observed no obvious abnormality in the morphology and intervals of the fluorescence puncta. Distribution of AZ protein marker SYD-2-GFP or UNC-10-GFP was not appreciably disturbed in *rimb-1* mutant axons, either. We also analyzed the localization of UNC-2, the α1 subunit of Ca$_v$2 VGCC. Transgenically expressed GFP-UNC-2 in D neurons displayed discrete punctate pattern along axons, overlapping with coexpressed SV marker mCherry-RAB-3 as reported (Fig. 2C; Saheki and Bargmann, 2009). In *rimb-1* mutants, the distribution pattern of GFP-UNC-2 puncta was the same as in wild type (Fig. 2D). There was no significant difference in the number of GFP-UNC-2 puncta between *rimb-1* mutants and wild type (Fig. 2F). In addition to this *rimb-1(gk452845)* nonsense allele, we tested a large deficiency allele *gkDf40*, which removed 200 kbp genomic region with 28 protein-coding genes including *rimb*-1. *gkDf40* homozygote animals were viable, and the distributions of SNB-1-GFP and GFP-UNC-2 in D neurons were also comparable to those of wild-type or the *rimb-1(gk452845)* mutants. Together these observations suggest that RIMB-1 is not essential for the presynaptic formation or the localization of UNC-2/Ca$_v$2. On the other hand, in the transgenic animals overexpressing RIMB-1, the number of GFP-UNC-2 puncta detected along neurites was significantly increased (Fig. 2E, F, one-way ANOVA: $F_{(2,43)} = 18.66$, $p < 0.0001$, *post hoc* Tukey–Kramer's tests: $p = 0.99$ for wild type vs *rimb-1*, $p < 0.0001$ for wild type vs *Ex[RIMB-1]*, $p < 0.0001$ for *rimb-1* vs *Ex[RIMB-1]*). As in wild type, GFP-UNC-2 puncta were found at the presynaptic sites marked with mCherry-RAB-3. This result suggests the possibility that increased expression of RIMB-1 proteins at presynaptic sites may recruit or stabilize more UNC-2/Ca$_v$2. Consistent with the possibility, the discrete puncta of GFP-UNC-2 were partially overlapped with FLAG-RIMB-1 puncta in immunostaining analysis (Fig. 2G). We tested whether the pan-neuronal RIMB-1 overexpression could enhance aldicarb sensitivity without UNC-2/Ca$_v$2 (Fig. 2H). *unc-2* loss-of-function mutants were more resistant to aldicarb treatment than wild type as reported (Miller et al., 1996). The RIMB-1 transgene enhanced aldicarb sensitivity in wild-type but not in *unc-2* background (Fig. 2H; log rank test, χ^2: 263.86, $p < 0.0001$, comparing each group, $p < 0.0001$ for wild type vs *Ex[RIMB-1]*, $p < 0.0001$ for wild type vs *unc-2*, $p < 0.0001$ for wild type vs *unc-2; Ex[RIMB-1]*, $p < 0.0001$ for *Ex[RIMB-1]* vs *unc-2*, $p < 0.0001$ for *Ex[RIMB-1]* vs *unc-2; Ex[RIMB-1]*, $p = 0.41$ for *unc-2* vs *unc-2; Ex[RIMB-1]*), suggesting that RIMB-1 could affect neuronal function through UNC-2/Ca$_v$2.

RIMB-1 and UNC-10/RIM redundantly regulate the presynaptic localization of UNC-2/Ca$_v$2

Presynaptic adaptor proteins exhibit extensive and specific interactions with each other (Südhof, 2012). Thus, we speculated that RIMB-1 functions redundantly with other presynaptic proteins

and examined a series of double loss-of-function mutants of *rimb-1* with genes that are known to function in presynaptic sites. We tested multiple CAZ proteins including SYD-2/Liprin-α, UNC-10/RIM, UNC-13/Munc13, and ELKS-1/ELKS/CAST, other regulators for presynaptic formation (RhoGAP-like protein SYD-1, ubiquitin E3 ligase RPM-1, serine/threonine kinase SAD-1) and synaptic transmission (UNC-2/Ca$_v$2 and the SNARE complex regulator UNC-18/Munc18), and other orthologs of mammalian VGCC binding proteins (MAGUK proteins LIN-2/CASK and LIN-10/Mint) as listed in Table 1. All these double mutants with *rimb-1* resembled corresponding single loss-of-function mutants for their locomotion on culture plates. In the comparisons of the localization patterns of presynaptic SV marker SNB-1-GFP in D neurons, no obvious difference was detected between each single and double mutant. Only in the detailed scoring of the number of puncta, several statistic differences were detected such that *sad-1; rimb-1* double mutant displayed slightly fewer puncta than wild type and *sad-1* single mutant (Table 1; one-way ANOVA: $F_{(3,41)} = 4.05$, $p < 0.013$, *post hoc* Tukey's tests: $p = 1.00$ for wild type vs *rimb-1*, $p = 0.99$ for wild type vs *sad-1*, $p = 0.041$ for wild type vs *rimb-1; sad-1*, $p = 0.99$ for *rimb-1* vs *sad-1*, $p = 0.051$ for *rimb-1* vs *rimb-1; sad-1*, $p = 0.019$ for *sad-1* vs *rimb-1; sad-1*), implying possible enhancement effects of *rimb-1*.

Analyses of presynaptic UNC-2 localization revealed more changes dependent on *rimb-1*. *rimb-1; unc-10* double mutants displayed significantly fewer presynaptic GFP-UNC-2 puncta than wild type or any of the single mutants in D neurons, whereas the localization of presynaptic marker mCherry-RAB-3 was indistinguishable among these strains (Fig. 3A–D). The number of GFP-UNC-2 puncta was reduced in *rimb-1; unc-10* double mutants by $\sim$60% compared with those in wild type, *rimb-1*, and *unc-10* single mutants (Fig. 3F; one-way ANOVA: $F_{(4,66)} = 42.14$, $p < 0.0001$, *post hoc* Tukey–Kramer's tests: $p = 1.00$ for wild type vs *rimb-1*, $p = 0.53$ for wild type vs *unc-10*, $p < 0.0001$ for wild type vs *rimb-1; unc-10*, $p = 0.47$ for *rimb-1* vs *unc-10*, $p < 0.0001$ for *rimb-1* vs *rimb-1; unc-10*, $p < 0.0001$ for *unc-10* vs *rimb-1; unc-10*). *rimb-1(gkDf40); unc-10* double mutants also showed decreased GFP-UNC-2 puncta, similar to the level of *rimb-1(gk452845); unc-10*. We next tested whether transgenic expression of RIMB-1 could rescue the GFP-UNC-2 defect in *rimb-1; unc-10* double mutants. Reduction of GFP-UNC-2 puncta in the double mutants was restored by pan-neuronal overexpression of RIMB-1a (7 of 7 transgenic lines rescued; Fig. 3E,F; Tukey–Kramer's tests: $p = 0.0001$ for wild type vs *rimb-1; unc-10; Ex[RIMB-1a]*, $p = 0.0003$ for *rimb-1* vs *rimb-1; unc-10; Ex[RIMB-1a]*, $p < 0.0001$ for *unc-10* vs *rimb-1; unc-10; Ex[RIMB-1a]*, $p < 0.0001$ for *rimb-1; unc-10* vs *rimb-1; unc-10; Ex[RIMB-1a]*) or RIMB-1b (2 of 2 lines rescued; Fig. 5E). Moreover, the number of puncta in the double mutant background was also restored after introducing the mCherry-RIMB-1a transgene expressing specifically in D neuron (Fig. 5I), suggesting that RIMB-1 regulates UNC-2/Ca$_v$2 localization in a cell-autonomous manner.

We further analyzed the effect of *rimb-1* genetic interaction for UNC-2/Ca$_v$2 localization in the bipolar sensory neurons AWC. AWC neurons reside in the lateral ganglia and form presynaptic inputs toward interneurons in the head (Fig. 4A; White et al., 1986). In wild type, GFP-UNC-2 clustered as multiple small puncta along the axon overlapping with mCherry-RAB-3 as reported (Fig. 4B; Saheki and Bargmann, 2009). In *rimb-1* mutants, GFP-UNC-2 was preserved at presynaptic sites of AWC as in wild type (Fig. 4C). Among the series of *rimb-1* double mutants, *rimb-1; unc-10* double mutants displayed severe defect of GFP-

UNC-2 localization. In *rimb-1; unc-10*, GFP-UNC-2 puncta in the axonal region were largely diminished, while mCherry-RAB-3 puncta in the same region or GFP-UNC-2 signals in cell bodies were not decreased (Fig. 4E). *unc-10* single mutants displayed normal GFP-UNC-2 localization pattern as reported (Fig. 4D; Saheki and Bargmann, 2009). We quantified GFP-UNC-2 puncta at the presynaptic region marked with mCherry-RAB-3. *rimb-1; unc-10* double mutants displayed >90% of reduction in the total area of GFP-UNC-2 puncta compared with wild type, whereas each *rimb-1* or *unc-10* single mutant showed no difference (Fig. 4K; one-way ANOVA: $F_{(3,36)}$ = 8.49, p = 0.0002, *post hoc* Tukey's tests: p = 0.99 for wild type vs *rimb-1*, p = 0.75 for wild type vs *unc-10*, p = 0.0009 for wild type vs *rimb-1; unc-10*, p = 0.58 for *rimb-1* vs *unc-10*, p = 0.0004 for *rimb-1* vs *rimb-1; unc-10*, p = 0.014 for *unc-10* vs *rimb-1; unc-10*). Both the number and average size of GFP-UNC-2 puncta were significantly reduced only in the double mutant (Fig. 4L,M; number, one-way ANOVA: $F_{(3,36)}$ = 6.18, p = 0.0017, *post hoc* Tukey's tests: p = 0.92 for wild type vs *rimb-1*, p = 1.00 for wild type vs *unc-10*, p = 0.0044 for wild type vs *rimb-1; unc-10*, p = 0.91 for *rimb-1* vs *unc-10*, p = 0.022 for *rimb-1* vs *rimb-1; unc-10*, p = 0.0038 for *unc-10* vs *rimb-1; unc-10*; average size, one-way ANOVA $F_{(3,36)}$ = 10.74, p < 0.0001, *post hoc* Tukey's tests: p = 0.75 for wild type vs *rimb-1*, p = 1.00 for wild type vs *unc-10*, p = 0.0010 for wild type vs *rimb-1; unc-10*, p = 0.84 for *rimb-1* vs *unc-10*, p < 0.0001 for *rimb-1* vs *rimb-1; unc-10*, p = 0.0006 for *unc-10* vs *rimb-1; unc-10*). On the other hand, there was no significant difference in the total fluorescent signals of GFP-UNC-2 in axonal process, which includes both punctate and weakly diffused signals (Fig. 4N; one-way ANOVA: $F_{(3,36)}$ = 1.08, p = 0.37, *post hoc* Tukey's tests: p = 0.96 for wild type vs *rimb-1*, p = 0.97 for wild type vs *unc-10*, p = 0.61 for wild type vs *rimb-1; unc-10*, p = 0.78 for *rimb-1* vs *unc-10*, p = 0.32 for *rimb-1* vs *rimb-1; unc-10*, p = 0.86 for *unc-10* vs *rimb-1; unc-10*). These results suggested that GFP-UNC-2 failed to be clustered as small puncta at the presynaptic sites but was more diffusely distributed along the axonal process in *rimb-1; unc-10* double mutant (Fig. 4O). This genetic interaction phenotype of *rimb-1* in AWC was also confirmed using *gkDf40* (Fig. 4F). *gkDf40; unc-10* double mutants displayed diminished presynaptic GFP-UNC-2 signal comparable to *rimb-1(gk452845); unc-10* (Fig. 4G; Table 1; one-way ANOVA: $F_{(3,36)}$ = 9.09, p = 0.0001, *post hoc* Tukey's tests: p =
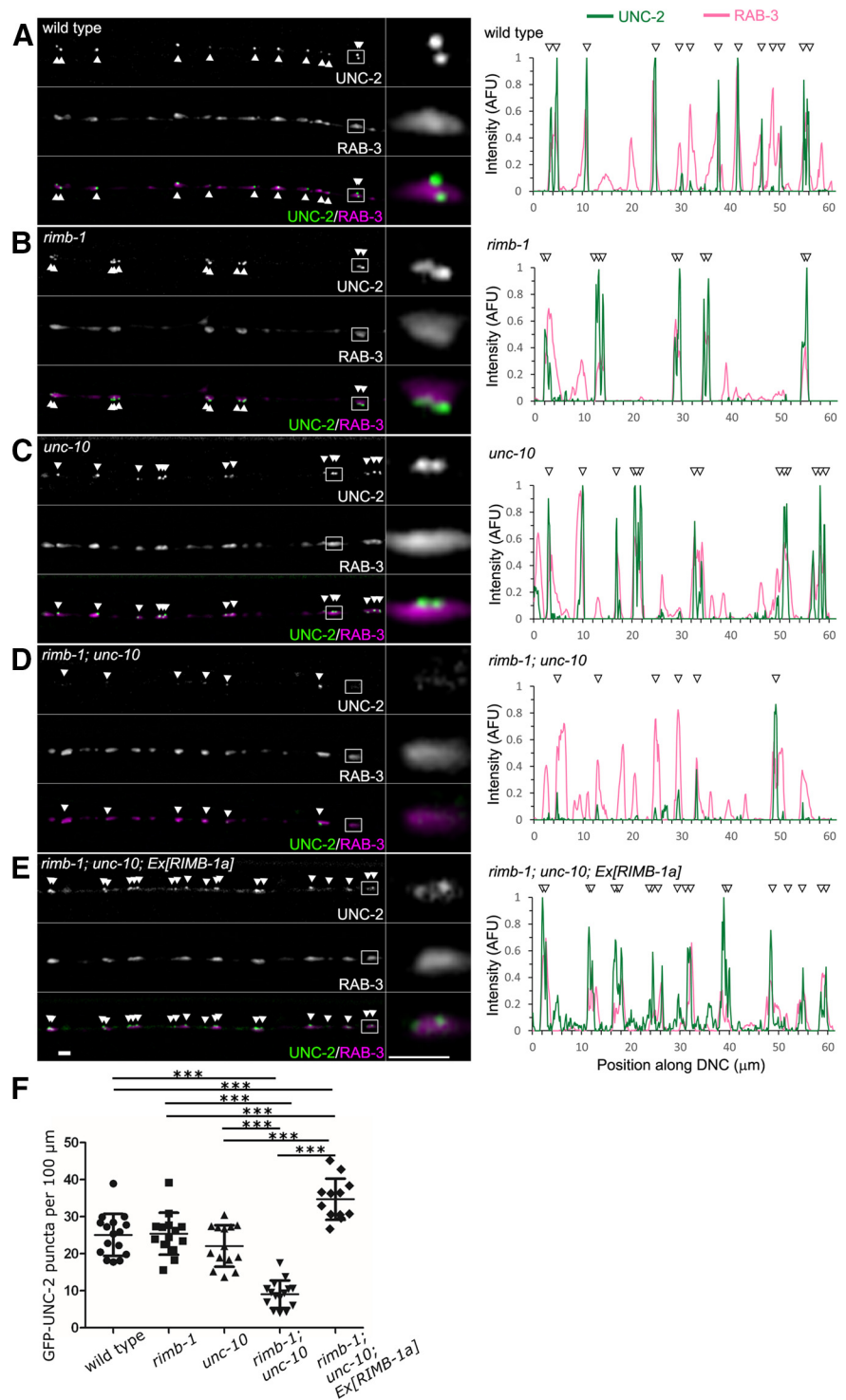
Figure 3. Presynaptic localization of UNC-2/Ca$_v$2 in D neurons was reduced in *rimb-1; unc-10/RIM* double mutants. **A–E**, Localization of GFP-UNC-2 coexpressed with presynaptic marker mCherry-RAB-3 in D neurons was analyzed in wild type (**A**), *rimb-1* (**B**), *unc-10* (**C**), *rimb-1; unc-10* (**D**) mutants, and *rimb-1; unc-10* with pan-neuronal transgenic expression of RIMB-1a (**E**). Representative fluorescent images of dorsal cords (left) and enlarged view of the boxed single presynaptic site (middle) accompanied with line scan intensity profiles along the axons (right charts) are shown. Arrowheads indicate GFP-UNC-2 colocalized with mCherry-RAB-3. Scale bars, 2 μm. **F**, Quantification of the number of GFP-UNC-2 puncta in D neurons. GFP-UNC-2 puncta were significantly fewer in *rimb-1; unc-10*, and pan-neuronal RIMB-1a expression restored the number. Mean ± SD, n = 12–16. Tukey–Kramer test following one-way ANOVA, ***p < 0.001.

0.88 for wild type vs *gkDf40*, p = 0.76 for wild type vs *unc-10*, p = 0.0012 for wild type vs *gkDf40; unc-10*, p = 0.33 for *gkDf40* vs *unc-10*, p = 0.0001 for *gkDf40* vs *gkDf40; unc-10*, p = 0.018 for *unc-10* vs *gkDf40; unc-10*). These observations indicate that
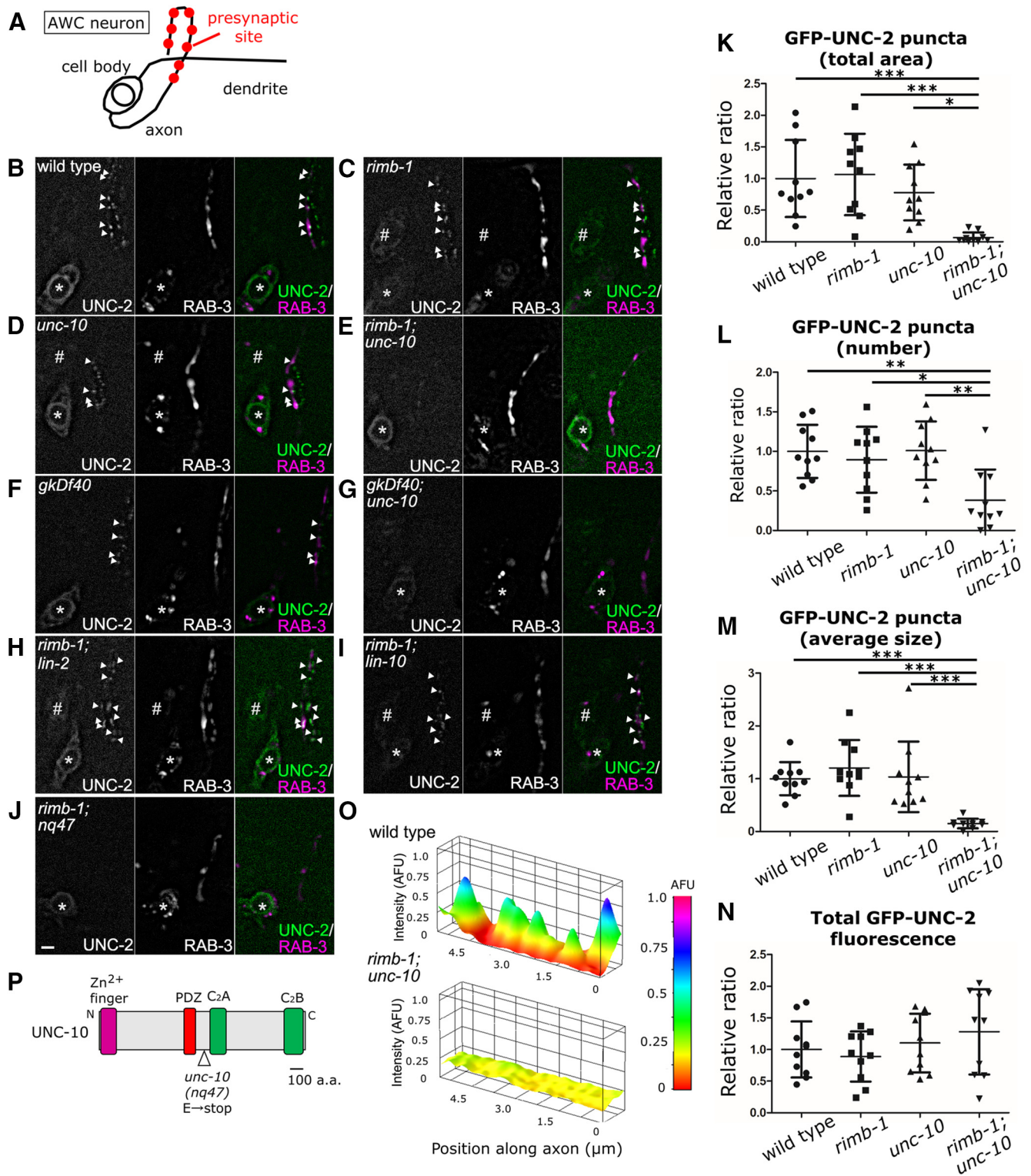
Figure 4. Presynaptic localization of UNC-2/Caᵥ2 in AWC neurons was impaired in *rimb-1; unc-10/RIM* double mutants. ***A***, Schematic drawing of AWC neuron. Presynaptic structures (red circles) are formed along the distal part of the axon. ***B–J***, Representative fluorescent images of GFP-UNC-2 coexpressed with mCherry-RAB-3 in AWC neurons in animals of indicated genotype. GFP-UNC-2 puncta colocalized with mCherry-RAB-3 along AWC axon (arrowheads) were disappeared in *rimb-1; unc-10* (***E***) and *gkDf40; unc-10* (***G***) double mutants. Asterisks and hashtags indicated AWC and AWB cell bodies, respectively. Scale bar, 2 μm. ***K–N***, Quantification of GFP-UNC-2 signals in AWC axon. Total area (***K***), number (***L***), and average size (***M***) of GFP-UNC-2 puncta and total GFP-UNC-2 fluorescence along the axons (***N***) were analyzed. All three parameters for GFP-UNC-2 puncta but not total GFP-UNC-2 fluorescence were significantly lower in *rimb-1; unc-10*. The values are indicated as a relative ratio to that in wild type (mean ± SD, $n = 10$). Tukey test following one-way ANOVA: $*p < 0.05$, $**p < 0.01$, $***p < 0.001$. ***O***, 3D heatmap representation of GFP-UNC-2 fluorescence intensity around presynaptic sites. GFP-UNC-2 was distributed punctately in wild type but diffusely in *rimb-1; unc-10*. ***P***, Schematic presentation of UNC-10 proteins. *unc-10(nq47)* allele identified in the genetic enhancer screen for *rimb-1* introduces a premature stop codon as indicated.

rimb-1 and *unc-10* have redundant roles in regulating UNC-2/Ca$_v$2 localization in AWC. The localization defect of GFP-UNC-2 in AWC neurons of *rimb-1; unc-10* was observed more apparently than that in D neurons.

The presynaptic distributions of GFP-UNC-2 in the other double mutants with *rimb-1* were not compromised either in D neurons or AWC neurons. We quantified GFP-UNC-2 signals in AWC neurons and detected no significant quantitative difference among wild type and each single and double mutant animal except for *rimb-1; unc-10* (Table 1). Distribution of presynaptic SV marker mCherry-RAB-3 in AWC was affected in various degrees in some single mutants and double mutants (Table 1), however, GFP-UNC-2 was still observed as distinct puncta adjacent to the disturbed presynaptic marker signals. Even in the double mutants of *rimb-1* with *lin-2/CASK*, *lin-10/Mint*, and *elks-1/ELKS*, which encode worm orthologs of mammalian VGCC binding proteins, did not display any apparent abnormality in the localization of GFP-UNC-2 in D neurons or AWC neurons (Fig. 4H,I). These results support a central role of RIMB-1 and UNC-10/RIM proteins in UNC-2/Ca$_v$2 localization.

In parallel with the candidate based double-mutant analysis, we performed an unbiased forward genetic screen in *rimb-1* background, using GFP-UNC-2 in AWC neuron, to search for molecules, which may play a redundant role with *rimb-1*. We isolated one recessive mutant *nq47*. *rimb-1; nq47* animals displayed compromised presynaptic localization of GFP-UNC-2 in D neurons or AWC neurons as *rimb-1; unc-10* did (Fig. 4J), and behaviorally also resembled *rimb-1; unc-10*. Indeed, genetic linkage and complementation analysis revealed this enhancer mutant *nq47* was an *unc-10* loss-of-function allele. *nq47* introduces a premature stop codon in the middle of the coding sequence, which would likely cause strong loss-of-function (Fig. 4P).

Together with the results from both candidate genetic interaction analysis and unbiased forward genetic screen, two presynaptic adaptor proteins, RIMB-1 and UNC-10/RIM, likely play redundant and critical function to regulate the abundance of UNC-2/Ca$_v$2 at presynaptic sites in neurons.

The C-terminal SH3 domain is essential for the function of RIMB-1

RIMB-1 is a multi-domain adaptor protein with three SH3 and two FN3 domains. To gain more mechanistic insights into RIMB-1 function, we generated a series of truncated constructs, including RIMB-1ΔN, which lacks the N-terminal region including the first SH3 and two FN3 domains, RIMB-1ΔC, which lacks the C-terminal half including the second and third SH3 domains, and RIMB-1ΔSH3-III, which lacks the C-terminal third SH3 domain (summarized in Fig. 5A).

We first tested the functional activity of these RIMB-1 constructs by transgenically expressing them under pan-neuronal promoter in *rimb-1; unc-10* double mutant background. We analyzed movement of multiple transgenic lines for every construct either on culture plate or in liquid and found that all RIMB-1 and RIMB-1ΔN but none of RIMB-1ΔC or RIMB-1ΔSH3-III transgenic lines recovered the movement defects of *rimb-1; unc-10* double mutant (Fig. 5A). We evaluated their motility by swimming assay and observed that RIMB-1 and RIMB-1ΔN restored the movement defects of *rimb-1; unc-10* double, but RIMB-1ΔC or RIMB-1ΔSH3-III failed to elevate reduced swimming motility (Fig. 5B; one-way ANOVA: $F_{(4,45)} = 112.77$, $p < 0.0001$, *post hoc* Dunnett's tests: $p < 0.0001$ for *rimb-1; unc-10* vs *rimb-1; unc-10; Ex[RIMB-1]*, $p < 0.0001$ for *rimb-1; unc-10* vs *rimb-1; unc-10; Ex[RIMB-1ΔN]*, $p = 0.9901$

for *rimb-1; unc-10* vs *rimb-1; unc-10; Ex[RIMB-1ΔC]*, $p = 0.48$ for *rimb-1; unc-10* vs *rimb-1; unc-10; Ex[RIMB-1ΔSH3-III]*). We also examined the effects of these transgenes on UNC-2/Ca$_v$2 localization in *rimb-1; unc-10* (Fig. 5A, C–H). Transgenic expression of RIMB-1, as well as RIMB-1ΔN, increased the number of GFP-UNC-2 puncta in the double mutants, in some cases, even more than wild-type animals (Fig. 5E,F). On the other hand, *rimb-1; unc-10* animals with RIMB-1ΔC and RIMB-1ΔSH3-III displayed only a few GFP-UNC-2 puncta, similar to the double mutants without any transgene (Fig. 5G,H). These results suggest that the third SH3 domain is essential for the RIMB-1 function.

To identify the domains in RIMB-1 required for its presynaptic localization, we tagged RIMB-1 truncated constructs with mCherry and coexpressed with presynaptic SV marker SNB-1-GFP in D neurons of wild-type animals. mCherry-RIMB-1 and RIMB-1ΔN were distributed as small puncta and colocalized with SNB-1-GFP along axons (Fig. 5J,K). mCherry-RIMB-1ΔSH3-III also displayed similar small punctate pattern overlapping with the SV marker (Fig. 5M), although RIMB-1ΔSH3-III lacks the rescue ability. mCherry-RIMB-1ΔC showed more diffused distribution, partly overlapping with SV marker (Fig. 5L), suggesting a requirement of the C-terminal region of RIMB-1 for its restricted localization to the small area within presynaptic sites.

Together these results revealed differential roles of multiple RIMB-1 domains for its localization and function. The third SH3 domain at the C-terminal end of RIMB-1 may not be critical for its presynaptic localization, however, is essential for the function of RIMB-1 including the regulation of the presynaptic localization of UNC-2/Ca$_v$2.

Precise localization of RIMB-1 at presynaptic sites requires UNC-2/Ca$_v$2

Precise localization of RIMB-1 at presynaptic sites is likely important for its function. We, therefore, explored the molecules required for the presynaptic localization of RIMB-1 by analyzing mCherry-RIMB-1 in D neurons together with SV marker SNB-1-GFP in several loss-of-function mutant backgrounds (Fig. 6). SYD-2/Liprin-α is a key protein for the presynaptic assembly (Zhen and Jin, 1999). In *syd-2* mutant, presynaptic structures were abnormal as observed as the disturbed distribution of SNB-1-GFP. However, the small punctate distribution of RIMB-1 and its colocalization with SNB-1-GFP were preserved (Fig. 6B). Next, we examined the requirement of RBP interactor homologs UNC-10/RIM and UNC-2/Ca$_v$2. In either *unc-10* or *unc-2*, mCherry-RIMB-1 was observed as small puncta along neurites within every punctum of SNB-1-GFP as in wild type (Fig. 6C,D, filled arrowhead), suggesting UNC-10/RIM or UNC-2/Ca$_v$2 is not an essential factor for the localization. However, in addition to such normally distributed puncta overlapping with the presynaptic marker in *unc-2* mutants, mCherry-RIMB-1 displayed many irregular punctate signals that were not colocalized with SNB-1-GFP (Fig. 6D, open arrowheads, F). This observation suggests the possibility that UNC-2/Ca$_v$2 is important to restrict RIMB-1 at presynaptic sites, although it is not a critical determinant for presynaptic localization of RIMB-1. Similar extra synaptic misdistribution of RIMB-1 was occasionally observed in *unc-10* but not in *syd-2* mutants (Fig. 6F), implying partial contribution of UNC-10/RIM to the restricted localization.

To further evaluate the role of presynaptic UNC-2/Ca$_v$2 for the localization of mCherry-RIMB-1, we examined the requirement of *calf-1*, which encodes an ER transmembrane protein essential for UNC-2/Ca$_v$2 trafficking from ER. In *calf-1* loss-of-
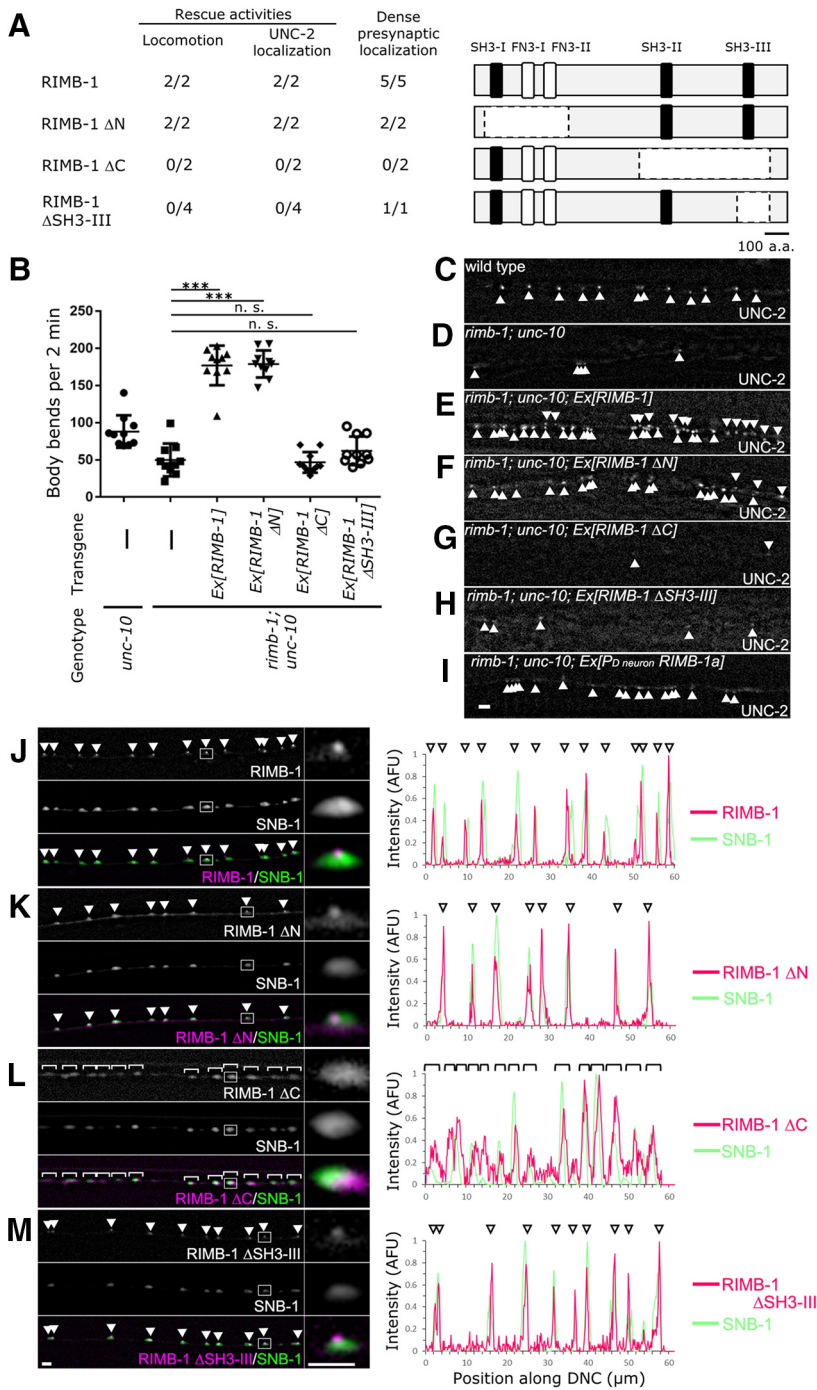
Figure 5. Structural-functional analysis of RIMB-1 revealed a functional requirement of the C-terminal SH3 domain. **A**, Schematic drawing of RIMB-1 deletion constructs and summary of the transgenic analyses. Rescue activities of pan-neuronally expressed constructs for locomotion and UNC-2 localization defects in *rimb-1; unc-10* double mutants, and the abilities of mCherry-tagged constructs expressed in D neurons for presynaptic localization were analyzed. The number of transgenic lines with the activities/abilities as a fraction of total lines analyzed is shown for each construct. **B**, Effect of pan-neuronal transgenic expression of RIMB-1 constructs on swimming motility. Mean ± SD, $n = 9–10$. Dunnett test following one-way ANOVA: n.s. $p \geq 0.05$, ***$p < 0.001$. **C–I**, Effect of transgenic expression of RIMB-1 constructs under pan-neuronal (**E–H**) or D neuron (**I**) promoter on the localization of GFP-UNC-2 (arrowheads) in D neurons. Representative fluorescent images of dorsal nerve cords in animals of indicated genotype are shown. RIMB-1 and RIMB-1ΔN recovered both motility and GFP-UNC-2 localization in *rimb-1; unc-10* mutants, but RIMB-1ΔC or RIMB-1ΔSH3-III did not. **J–M**, Localization of mCherry-RIMB-1 constructs coexpressed with SNB-1-GFP in D neurons. Representative fluorescent images of dorsal cords (left) and enlarged view of the boxed single presynaptic site (middle) accompanied with line scan intensity profiles along the axons (right charts) are shown. mCherry-RIMB-1, RIMB-1ΔN, and RIMB-1ΔSH3-III were regularly distributed as small dense puncta at presynaptic sites (**J, K, M**, arrowheads), but RIMB-1ΔC displayed more widely diffused puncta (**L**, brackets). Scale bars, 2 μm.

function animals, UNC-2/Caᵥ2 failed to distribute along neurites but retained in cell bodies as reported (Saheki and Bargmann, 2009). On the other hand, mCherry-RIMB-1 was able to be distributed along neurites as discrete puncta (Fig. 6E), implying that the trafficking process of RIMB-1 from cell bodies is independent of that of UNC-2/Caᵥ2. However, in addition to the presynaptic RIMB-1 puncta colocalized with SNB-1-GFP (Fig. 6E, filled arrowheads), all *calf-1* animals displayed an irregular extrasynaptic distribution of mCherry-RIMB-1 resembling the misdistribution in *unc-2* mutant (Fig. 6E, open arrowheads, F). Together, these results suggest that presynaptic UNC-2/Caᵥ2 is involved in the precise localization of RIMB-1 limited to presynaptic sites.

Discussion

The presynaptic AZ is a highly organized structure for neurotransmitter release, and how CAZ adaptor proteins assemble and regulate VGCC and other molecules has been an important question. In this study, we focused on *C. elegans* RIMB-1, an ortholog of CAZ protein RBPs. Our genetic analysis revealed a redundant function of RIMB-1 and UNC-10/RIM to regulate the abundance of presynaptic clusters of UNC-2/Caᵥ2 and provided mechanistic insights into RIMB-1 localization and function.

Presynaptic localization of UNC-2/Caᵥ2 clusters depends on redundant action of RIMB-1 and UNC-10/RIM in *C. elegans*

Precise localization of UNC-2/Caᵥ2 at presynaptic AZ is critical for synaptic transmission, however, presynaptic molecules necessary for the localization had remained unknown in worms. In the *rimb-1; unc-10* double loss-of-function mutants, the abundance of UNC-2/Caᵥ2 clusters at presynaptic sites was severely compromised in D-type motor and AWC sensory neurons, whereas neither *rimb-1* nor *unc-10* single mutant displayed such obvious defect (Figs. 3, 4). Conversely, pan-neuronal overexpression of RIMB-1 in wild-type background increased the abundance of presynaptic clusters of UNC-2/Caᵥ2 (Fig. 2E, F) and rescued the defect in *rimb-1; unc-10* double mutants (Figs. 3F, 5E). Thus, neuronal RIMB-1 is a key molecule that positively regulates UNC-2/Caᵥ2 clusters at presynaptic sites.

RIM family is critical for neurotransmitter release and AZ formation (Y. Wang et al., 1997; Acuna et al., 2016; S. S. H.
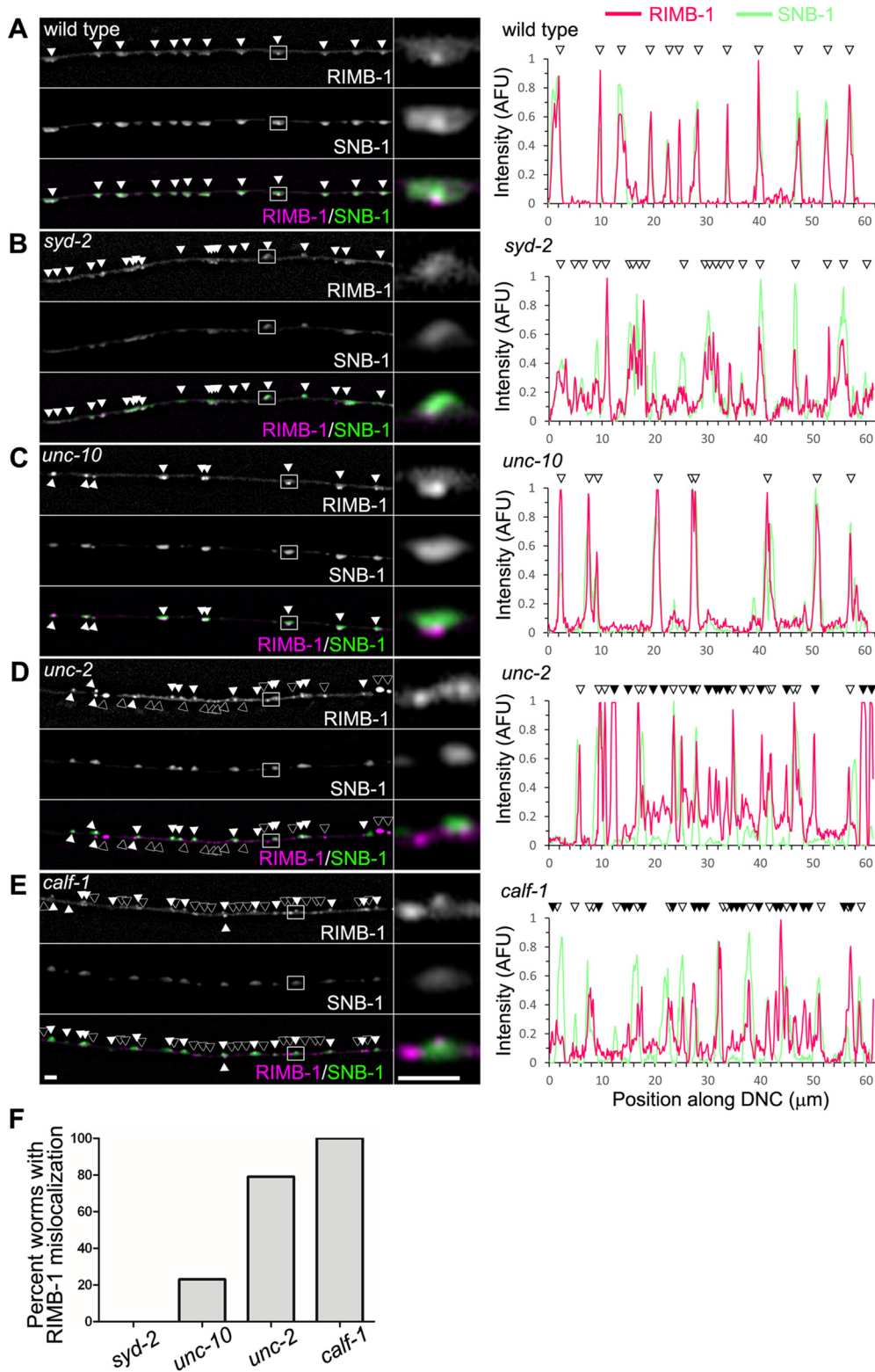
Figure 6. Restricted localization of RIMB-1 was impaired in the absence of presynaptic UNC-2/Ca$_v$2. **A–E**, Localization of mCherry-RIMB-1 coexpressed with SNB-1-GFP in D neurons was analyzed in wild type (**A**), *syd-2* (**B**), *unc-10* (**C**), *unc-2* (**D**), and *calf-1* (**E**) mutants. Representative fluorescent images of dorsal nerve cords (left) and enlarged views of the boxed regions (middle) accompanied with line scan intensity profiles along the axons (right charts) are shown. mCherry-RIMB-1 overlapping and non-overlapping with SNB-1-GFP are marked with filled and open arrowheads, respectively. Scale bars, 2 μm. **F**, Penetrance of the RIMB-1 mislocalization phenotype. Percentage of worms with irregular mCherry-RIMB-1 puncta non-overlapping with SNB-1-GFP was scored ($n = 11$–41).

Wang et al., 2016) and directly binds and regulates Ca$_v$2 in mice (Han et al., 2011; Kaeser et al., 2011). Worm homolog UNC-10 is also required for the localization of SV at AZ and normal synaptic transmission (Koushika et al., 2001; Stigloher et al., 2011), how-

ever, the presynaptic UNC-2/Ca$_v$2 localization was intact in *unc-10* single mutant (Saheki and Bargmann, 2009). Our characterization of RIMB-1 has revealed functional redundancy with UNC-10/RIM for regulating UNC-2/Ca$_v$2.

RIMB-1 colocalizes with UNC-2/Ca$_v$2 as well as UNC-10/RIM (Figs. 1H, 2G). Partial overlap between the localization of RIMB-1 and UNC-2/Ca$_v$2 at presynaptic sites was observed under super-resolution (Kurshan et al., 2018). As RIMB-1 and UNC-10 are homologs of Ca$_v$2 binding proteins, a simple mechanistic explanation may be that these two proteins anchor and stabilize UNC-2/Ca$_v$2 at the presynaptic sites. Multiple SH3 domains of RBPs can bind Ca$_v$2, but the third SH3 has the highest affinity (Hibino et al., 2002; K. S. Liu et al., 2011; Siebert et al., 2015; Wu et al., 2019). The requirement of the third SH3 domain of RIMB-1 for UNC-2/Ca$_v$2 localization in our structural-functional analysis supports evolutionary conservation (Fig. 5H).

VGCC also binds other proteins, in addition to RBP and RIM. In our systematic double mutant analysis, double mutants of other VGCC binding protein homologs such as LIN-2/CASK, LIN-10/Mint, and ELKS-1/ELKS did not display any notable UNC-2/Ca$_v$2 defect (Fig. 4H,I; Table 1). In addition, in our forward genetic screen, we only identified *nq47*, a loss-of-function allele of *unc-10*, as a strong enhancer of *rimb-1* mutant. Therefore, it is conceivable that RIMB-1 and UNC-10/RIM redundantly play a central role for the UNC-2/Ca$_v$2 localization commonly in worm neurons, although additional contributions of other factors cannot be ruled out.

rimb-1 single mutants displayed mild defects in motility and aldicarb sensitivity (Fig. 2A,B). Conversely, pan-neuronal RIMB-1 overexpression upregulated swimming motility in *rimb-1* mutants and enhanced aldicarb sensitivity (Figs. 2A,B, 5B). Although a recent electrophysiological study reported that spontaneous neurotransmitter release at both cholinergic and GABAergic synapses was normal in *rimb-1* mutants (H. Liu et al., 2018), these observations suggest that RIMB-1 is positively involved in synaptic function to some extent. Because enhanced aldicarb sensitivity by RIMB-1 overexpression was lost in *unc-2* loss-of-function background (Fig. 2H), UNC-2/Ca$_v$2 may partly mediate the effect of RIMB-1 on neuronal function.

Conserved roles of RBP in the regulation of VGCC Ca$_v$2
Our analysis on *C. elegans* RIMB-1 has revealed common importance of RBPs for the regulation of presynaptic Ca$_v$2 in multiple organisms together with some diversities. In mice, RBP is likely more essential for fine-tuning of VGCC localization within AZ and function than for its gross presynaptic abundance (Acuna et al., 2015; Grauel et al., 2016). RIM may play a central role for the presynaptic Ca$_v$2 abundance in combination with RBP, because loss of RIMs reduced presynaptic Ca$_v$2 protein and calcium entry (Han et al., 2011; Kaeser et al., 2011), and co-depletion of RIMs with RBPs and ELKS severely impaired presynaptic VGCC function and reduced presynaptic Ca$_v$2 (Acuna et al., 2016; S. S. H. Wang et al., 2016). In *Drosophila*, every single mutants of RBP (K. S. Liu et al., 2011), RIM (Graf et al., 2012), Fife/RIM-Piccolo homolog (Bruckner et al., 2017), and Bruchpilot/ELKS-like protein (Kittel et al., 2006) displayed the reduction of presynaptic Cac/Ca$_v$2 proteins abundance as well as its function at the neuromuscular junction. In *C. elegans*, the abundance of UNC-2/Ca$_v$2 at presynaptic sites was comparable among wild type, *rimb-1* and *unc-10* single mutants, but was strikingly reduced in *rimb-1; unc-10* double mutants (Figs. 3, 4). As for ELKS, either *elks-1* single, *rimb-1; elks-1*, or *unc-10; elks-1* double mutants did not display such UNC-2 localization defect (Table 1). Therefore, in worms, the highly redundant function of RIMB-1/RBP and UNC-10/RIM for the presynaptic localization of Ca$_v$2 is one of the characteristic features.

In mice and flies, loss of RBPs caused presynaptic assembly defect. RBP-null mutants in *Drosophila* displayed severe mislocalization of AZ proteins and cytomatrix structure at the neuromuscular junction (K. S. Liu et al., 2011). In mice, although depletion of RBPs alone caused no presynaptic structural change (Acuna et al., 2015; Grauel et al., 2016), co-depletion of RBPs and RIMs caused reduction of CAZ proteins, SV tethering, and dense projections at presynaptic sites (Acuna et al., 2016). On the other hand, in *C. elegans*, single *rimb-1* mutant, either a nonsense mutation or a complete deletion, had no obvious defect in the localization of SV and AZ protein markers in D neurons. Recent analyses in cholinergic motor neurons of *rimb-1* mutant have identified slight defect for the distribution of SV and dense core vesicles, suggesting a minor contribution of RIMB-1 (Edwards et al., 2018; Morrison et al., 2018). In our double-mutant analyses, *rimb-1* did not cause strong enhancement or suppression effect on the distribution of SV proteins. Quantitative analyses detected a possibility of weak enhancement effect of *rimb-1* on some synaptic mutants such as *sad-1* (Table 1), implying that RIMB-1 is involved in normal presynaptic organization together with other presynaptic molecules. *rimb-1; unc-10* double mutant displayed no apparent abnormality in the distribution of presynaptic markers (Figs. 3, 4; Table 1). Thus, it rules out the possibility that UNC-2/Ca$_v$2 defect was secondary due to compromised presynaptic structure. Therefore, we consider that RIMB-1 may play a more essential role in the regulation of UNC-2/Ca$_v$2 rather than in the formation of basal presynaptic structure in worms.

Molecular mechanisms of RIMB-1 localization and function
RIMB-1 is predominantly localized at presynaptic sites highly overlapping with AZ proteins as observed for RBPs in other organisms (Fig. 1G,H), yet the anchoring machinery of RIMB-1 to presynaptic sites remains unclear. We found that RIMB-1 was apparently mislocalized out of presynaptic regions along neurites in addition to the normal small punctate presynaptic localization in the absence of presynaptic UNC-2/Ca$_v$2 (Fig. 6D–F). *unc-10* mutants also displayed extra-presynaptic localization at low penetrance (Fig. 6F). These observations suggest that the restriction of RIMB-1 localization to the presynaptic region requires UNC-2/Ca$_v$2, and partly UNC-10/RIM. Thus, it is likely that the requirement of RIMB-1 and UNC-2/Ca$_v$2 for their localization is bidirectional.

The C-terminal region of RIMB-1 including two SH3 domains is required for the precise localization within presynaptic sites (Fig. 5L). Either the N-terminal or C-terminal half of RIMB-1 was sufficient for its distribution around presynaptic sites (Fig. 5K,L). In addition to VGCCα1 and RIMs, RBPs interact with multiple proteins such as Bassoon and APLIP1/DJIP-1 (Davydova et al., 2014; Siebert et al., 2015). The localization of RIMB-1 could be attributed to redundant protein interactions through multiple domains with single or multiple anchor protein. The SH3 domains of RBP and RIM form condensed assembly through liquid-liquid phase separation to cluster VGCCα1 *in vitro*, and VGCCα1 can reciprocally promote the condensed assembly (Wu et al., 2019). Such dynamic interaction via multiple binding domains could also be involved in the bidirectional regulation between RIMB-1/RBP and UNC-2/Ca$_v$2 in *C. elegans*. Further investigating the functional contribution of the dynamic co-assembly *in vivo* using model animals will be important to dissect the redundancy between RIMB-1/RBP and UNC-10/RIM.

In conclusion, we find that RIMB-1 acts redundantly with UNC-10/RIM to regulate the abundance of presynaptic UNC-2/Ca$_V$2 in *C. elegans*. Moreover, there may be bidirectional regulation between RIMB-1 and UNC-2/Ca$_V$2 for their precise localizations. Genome-wide analyses of exonic variants in families with autism implicate an association of RBPs and RIM (Bucan et al., 2009; Krumm et al., 2015). Mutations in Ca$_V$2.1 gene *CACNA1A* cause familial neuronal disorders such as familial hemiplegic migraine-1 and episodic ataxia (for review, see Heyes et al., 2015). Therefore, to understand the whole picture of complex regulatory machinery involving RBP, RIM, and VGCC for clinical perspectives, studies using multiple model animals including *C. elegans* will provide valuable insights.

References

Ackermann F, Waites CL, Garner CC (2015) Presynaptic active zones in invertebrates and vertebrates. EMBO Rep 16:923–938.

Acuna C, Liu X, Gonzalez A, Südhof TC (2015) RIM-BPs mediate tight coupling of action potentials to Ca²⁺-triggered neurotransmitter release. Neuron 87:1234–1247.

Acuna C, Liu X, Südhof TC (2016) How to make an active zone: unexpected universal functional redundancy between RIMs and RIM-BPs. Neuron 91:792–807.

Brenner S (1974) The genetics of *Caenorhabditis elegans*. Genetics 77:71–94.

Bruckner JJ, Zhan H, Gratz SJ, Rao M, Ukken F, Zilberg G, O'Connor-Giles KM (2017) Fife organizes synaptic vesicles and calcium channels for high-probability neurotransmitter release. J Cell Biol 216:231–246.

Bucan M, Abrahams BS, Wang K, Glessner JT, Herman EI, Sonnenblick LI, Alvarez Retuerto AI, Imielinski M, Hadley D, Bradfield JP, Kim C, Gidaya NB, Lindquist I, Hutman T, Sigman M, Kustanovich V, Lajonchere CM, Singleton A, Kim J, Wassink TH, et al. (2009) Genome-wide analyses of exonic copy number variants in a family-based study point to novel autism susceptibility genes. PLoS Genet 5:e1000536.

Caylor RC, Jin Y, Ackley BD (2013) The *Caenorhabditis elegans* voltage-gated calcium channel subunits UNC-2 and UNC-36 and the calcium-dependent kinase UNC-43/CaMKII regulate neuromuscular junction morphology. Neural Dev 8:10.

Davydova D, Marini C, King C, Klueva J, Bischof F, Romorini S, Montenegro-Venegas C, Heine M, Schneider R, Schröder MS, Altrock WD, Henneberger C, Rusakov DA, Gundelfinger ED, Fejtova A (2014) Bassoon specifically controls presynaptic P/Q-type Ca²⁺ channels via RIM-binding protein. Neuron 82:181–194.

Dresbach T, Qualmann B, Kessels MM, Garner CC, Gundelfinger ED (2001) The presynaptic cytomatrix of brain synapses. Cell Mol Life Sci 58:94–116.

Edwards SL, Morrison LM, Manning L, Stec N, Richmond JE, Miller KG (2018) Sentryn acts with a subset of active zone proteins to optimize the localization of synaptic vesicles in *Caenorhabditis elegans*. Genetics 210:947–968.

Finney M, Ruvkun G (1990) The unc-86 gene product couples cell lineage and cell identity in *C. elegans*. Cell 63:895–905.

Graf ER, Valakh V, Wright CM, Wu C, Liu Z, Zhang YQ, DiAntonio A (2012) RIM promotes calcium channel accumulation at active zones of the *Drosophila* neuromuscular junction. J Neurosci 32:16586–16596.

Grauel MK, Maglione M, Reddy-Alla S, Willmes CG, Brockmann MM, Trimbuch T, Rosenmund T, Pangalos M, Vardar G, Stumpf A, Walter AM, Rost BR, Eickholt BJ, Haucke V, Schmitz D, Sigrist SJ, Rosenmund C (2016) RIM-binding protein 2 regulates release probability by fine-tuning calcium channel localization at murine hippocampal synapses. Proc Natl Acad Sci U S A 113:11615–11620.

Han Y, Kaeser PS, Südhof TC, Schneggenburger R (2011) RIM determines Ca²⁺ channel density and vesicle docking at the presynaptic active zone. Neuron 69:304–316.

Heyes S, Pratt WS, Rees E, Dahimene S, Ferron L, Owen MJ, Dolphin AC (2015) Genetic disruption of voltage-gated calcium channels in psychiatric and neurological disorders. Prog Neurobiol 134:36–54.

Hibino H, Pironkova R, Onwumere O, Vologodskaia M, Hudspeth AJ, Lesage F (2002) RIM binding proteins (RBPs) couple Rab3-interacting molecules (RIMs) to voltage-gated Ca²⁺ channels. Neuron 34:411–423.

Kaeser PS, Deng L, Wang Y, Dulubova I, Liu X, Rizo J, Südhof TC (2011) RIM proteins tether Ca²⁺ channels to presynaptic active zones via a direct PDZ-domain interaction. Cell 144:282–295.

Kittel RJ, Wichmann C, Rasse TM, Fouquet W, Schmidt M, Schmid A, Wagh DA, Pawlu C, Kellner RR, Willig KI, Hell SW, Buchner E, Heckmann M, Sigrist SJ (2006) Bruchpilot promotes active zone assembly, Ca²⁺ channel clustering, and vesicle release. Science 312:1051–1054.

Kiyonaka S, Nakajima H, Takada Y, Hida Y, Yoshioka T, Hagiwara A, Kitajima I, Mori Y, Ohtsuka T (2012) Physical and functional interaction of the active zone protein CAST/ERC2 and the β-subunit of the voltage-dependent Ca²⁺ channel. J Biochem 152:149–159.

Koushika SP, Richmond JE, Hadwiger G, Weimer RM, Jorgensen EM, Nonet ML (2001) A post-docking role for active zone protein rim. Nat Neurosci 4:997–1005.

Krumm N, Turner TN, Baker C, Vives L, Mohajeri K, Witherspoon K, Raja A, Coe BP, Stessman HA, He ZX, Leal SM, Bernier R, Eichler EE (2015) Excess of rare, inherited truncating mutations in autism. Nat Genet 47:582–588.

Kurshan PT, Merrill SA, Dong Y, Ding C, Hammarlund M, Bai J, Jorgensen EM, Shen K (2018) γ-Neurexin and Frizzled mediate parallel synapse assembly pathways antagonized by receptor endocytosis. Neuron 100:150–166.e4.

Liu H, Li L, Wang W, Gong J, Yang X, Hu Z (2018) Spontaneous vesicle fusion is differentially regulated at cholinergic and GABAergic synapses. Cell Rep 22:2334–2345.

Liu KS, Siebert M, Mertel S, Knoche E, Wegener S, Wichmann C, Matkovic T, Muhammad K, Depner H, Mettke C, Bückers J, Hell SW, Müller M, Davis GW, Schmitz D, Sigrist SJ (2011) RIM-binding protein, a central part of the active zone, is essential for neurotransmitter release. Science 334:1565–1569.

Macosko EZ, Pokala N, Feinberg EH, Chalasani SH, Butcher RA, Clardy J, Bargmann CI (2009) A hub-and-spoke circuit drives pheromone attraction and social behaviour in *C. elegans*. Nature 458:1171–1175.

Mathews EA, García E, Santi CM, Mullen GP, Thacker C, Moerman DG, Snutch TP (2003) Critical residues of the *Caenorhabditis elegans* unc-2 voltage-gated calcium channel that affect behavioral and physiological properties. J Neurosci 23:6537–6545.

Maximov A, Südhof TC, Bezprozvanny I (1999) Association of neuronal calcium channels with modular adaptor proteins. J Biol Chem 274:24453–24456.

Mello CC, Kramer JM, Stinchcomb D, Ambros V (1991) Efficient gene transfer in *C. elegans*: extrachromosomal maintenance and integration of transforming sequences. EMBO J 10:3959–3970.

Miller KG, Alfonso A, Nguyen M, Crowell JA, Johnson CD, Rand JB (1996) A genetic selection for *Caenorhabditis elegans* synaptic transmission mutants. Proc Natl Acad Sci U S A 93:12593–12598.

Morrison LM, Edwards SL, Manning L, Stec N, Richmond JE, Miller KG (2018) Sentryn and SAD kinase link the guided transport and capture of dense core vesicles in *Caenorhabditis elegans*. Genetics 210:925–946.

Müller M, Genç Ö, Davis GW (2015) RIM-binding protein links synaptic homeostasis to the stabilization and replenishment of high release probability vesicles. Neuron 85:1056–1069.

Nguyen M, Alfonso A, Johnson CD, Rand JB (1995) *Caenorhabditis elegans* mutants resistant to inhibitors of acetylcholinesterase. Genetics 140:527–535.

Saheki Y, Bargmann CI (2009) Presynaptic CaV2 calcium channel traffic requires CALF-1 and the α2δ subunit UNC-36. Nat Neurosci 12:1257–1265.

Schafer WR, Kenyon CJ (1995) A calcium-channel homologue required for adaptation to dopamine and serotonin in *Caenorhabditis elegans*. Nature 375:73–78.

Schoch S, Gundelfinger ED (2006) Molecular organization of the presynaptic active zone. Cell Tissue Res 326:379–391.

Siebert M, Böhme MA, Driller JH, Babikir H, Mampell MM, Rey U, Ramesh N, Matkovic T, Holton N, Reddy-Alla S, Göttfert F, Kamin D, Quentin C, Klinedinst S, Andlauer TF, Hell SW, Collins CA, Wahl MC, Loll B, Sigrist S (2015) A high affinity RIM-binding protein/Aplip1 interaction prevents the formation of ectopic axonal active zones. eLife 4:e06935.

Simms BA, Zamponi GW (2014) Neuronal voltage-gated calcium channels: structure, function, and dysfunction. Neuron 82:24–45.

Stigloher C, Zhan H, Zhen M, Richmond J, Bessereau JL (2011) The presynaptic dense projection of the *Caenorhabditis elegans* cholinergic neuromuscular junction localizes synaptic vesicles at the active zone through SYD-2/Liprin and UNC-10/RIM-dependent interactions. J Neurosci 31:4388–4396.

Südhof TC (2012) The presynaptic active zone. Neuron 75:11–25.

Taru H, Jin Y (2011) The Liprin homology domain is essential for the homomeric interaction of SYD-2/Liprin-α protein in presynaptic assembly. J Neurosci 31:16261–16268.

Wang SSH, Held RG, Wong MY, Liu C, Karakhanyan A, Kaeser PS (2016) Fusion competent synaptic vesicles persist upon active zone disruption and loss of vesicle docking. Neuron 91:777–791.

Wang Y, Okamoto M, Schmitz F, Hofmann K, Südhof TC (1997) Rim is a putative Rab3 effector in regulating synaptic-vesicle fusion. Nature 388:593–598.

Wang Y, Sugita S, Südhof TC (2000) The RIM/NIM family of neuronal C2 domain proteins: interactions with Rab3 and a new class of src homology 3 domain proteins. J Biol Chem 275:20033–20044.

White JG, Southgate E, Thomson JN, Brenner S (1986) The structure of the nervous system of the nematode *Caenorhabditis elegans*. Philos Trans R Soc Lond B Biol Sci 314:1–340.

Wu X, Cai Q, Shen Z, Chen X, Zeng M, Du S, Zhang M (2019) RIM and RIM-BP form presynaptic active-zone-like condensates via phase separation. Mol Cell 73:971–984.e5.

Zhen M, Jin Y (1999) The Liprin protein SYD-2 regulates the differentiation of presynaptic termini in *C. elegans*. Nature 401:371–375.